ADAPTIVE PARTICLE ENCAPSULATION USING DIGITAL OPTO-FLUIDIC
LITHOGRAPHY

By

MANISH BOORUGU

A thesis submitted to the

School of Graduate Studies

Rutgers, The State University of New Jersey

In partial fulfillment of the requirements

For the degree of

Master of Science

Graduate Program in Mechanical and Aerospace Engineering

Written under the direction of

Howon Lee

And approved by

_____

_____

_____

_____

New Brunswick, New Jersey

January 2018

ABSTRACT OF THE THESIS

Adaptive Particle Encapsulation Using Digital Opto-Fluidic Lithography

By Manish Boorugu

Thesis Director:

Howon Lee

Encapsulation of living cells using microgels has a wide range of applications in pharmaceutical research, tissue engineering, regenerative medicine, and personalized drug screening. Various cell encapsulation techniques have been proposed thus far focusing on creating cell-laden microgel particles. However, current techniques have limited control over the shape and size of the encapsulating particles and lack ability to address individual cells.

This research aims to develop a method for adaptive encapsulation of particles with geometrically and biochemically complex micro-particles. To this end, we demonstrate image-based particle detection in a microfluidic channel and real-time in-flow lithography to encapsulate suspended particle employing a digital micro display as a dynamically reconfigurable virtual photomask. Digital dynamic mask is economical and offers the flexibility of rapidly changing the mask on demand. Microfluidic environment allows for mass production of micro-particles having various chemical composition in a continuous manner. Combining these unique capabilities, we present encapsulation of individual

particles with graphically encoded information. Visual information (shape, size, and location) of polystyrene micro-beads suspended in a photo-curable liquid resin is acquired through digital imaging and subsequent image analysis, based on which desired digital patterns, possibly with graphical information, are created and optically projected on the target beads for lithographical in-flow encapsulation.

The work presented in this thesis provides a new method for particle encapsulation, which has the potential to lead to a breakthrough solution in pharmaceutical engineering, cancer research, and tissue engineering.

ACKNOWLEDGEMENTS

I would like to thank my advisor Prof. Howon Lee for giving me an opportunity to work with him. His continuous support and guidance has helped me immensely in the research process.

I would also like to thank rest of my thesis committee, Dr.German Drazer, Dr.Prosenjit Bagchi and Dr.Mehdi Javanmard for their willingness to join my thesis committee and the valuable time they took out of their schedule to review my thesis.

Many thanks to my amazing lab mates Chen Yang, Daehoon Han, Ridhish Morde and Zhaocheng Lu, who have been great to work with and for their help at various points of my research. In addition, many thanks to all the undergraduate students working in our lab who have made my time in the lab a fun experience.

Many thanks to my manager Robin Whittington-Easter, my friends Nicole Sciacchitano and David Gifford for sharing their advice towards career and life, which helped me immensely during my research and made my life easy in The United States.

Most importantly, I would like to thank my parents and my brother for their love and continuous support throughout college education. My parents and my brother have been amazingly supportive throughout this whole process, without which I would not be able to have completed my college education.

Table of Contents

List of Tables

List of Illustrations

1 Introduction

1.1 Background

In the past decade, synthesis and application of polymeric micro-particles has witnessed drastic advancements. Dispersions of polymeric particles are currently used commonly to provide effective protection, binding, and finishing to a number of industrial products such as paper, metals, and wood [1]. Gradually, polymeric particles have also found use in high value biological and analytical applications such as column supports for chromatography, beads for flow cytometry and in the recovery of Deoxyribonucleic Acid (DNA) and Proteins. The use of polymeric particles has grown from applications requiring bulk quantities of particles to niche applications in photonics, diagnostics and tissue engineering where properties of individual particles are critical due to their technological function [2]. At present, the most common method to synthesize polymeric particles of colloidal length scale in large volumes is emulsion polymerization technique and the prominent shape achieved with this process is a sphere [2]. Although spherical shapes are sufficient and desired for many applications, there has been a growing demand for custom designed and non-spherical particles in applications such as photonic crystals, chromatography and liquid crystal spacers [2][3]. The synthesis of particles required for these applications using the existing emulsion polymerization technique is expensive and time consuming.
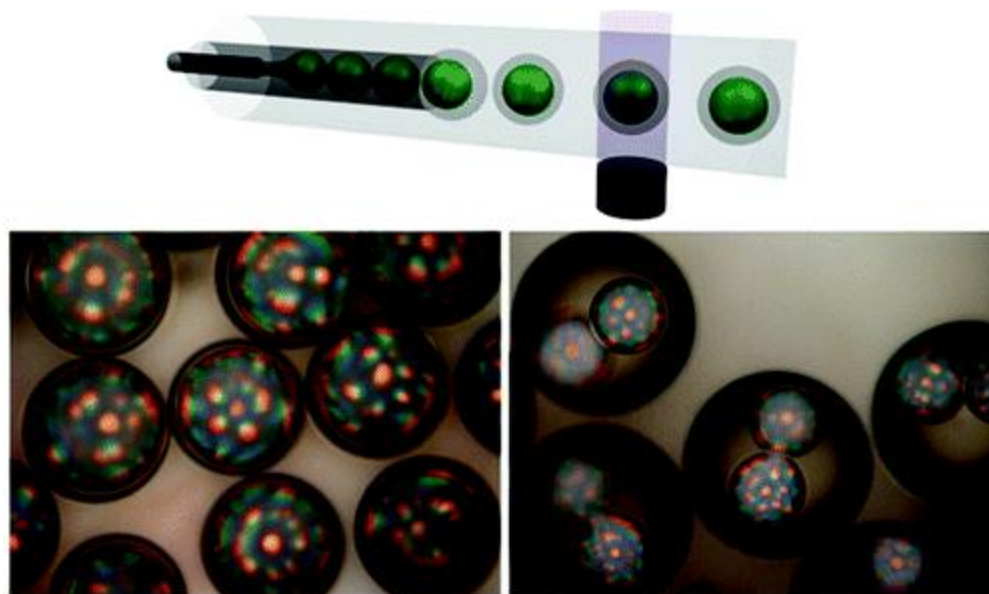
Figure 1.1: a) Schematic of opto-fluidic encapsulation of CCAs with micro capillary device and UV irradiation. b) Optical microscope images of SCCAs confined in polymeric shells dispersed in water phase [3].

To respond to the need of non-spherical particles, new techniques that are based on microfluidics have been developed. Polymeric particle synthesis using microfluidics can be broadly classified into droplet-based, multiphase methods and photolithography based methods. Inspired by the concept of membrane emulsification, in 1997 Nakajima group first demonstrated the controlled formation of micrometer-sized oil-in-water and water-in-oil emulsion droplets in a micro-machined silicone device [4]. Followed by the work on microchannel emulsification using a membrane inspired approach new methods for generated droplets were developed. In 2001, the Quake group developed a method to generate droplets using a T-junction microchannel [5]. The Stone group first implemented a planar flow-focusing device geometry in a microfluidic device to form droplets in a controlled manner in 2003 [6]. Later Seong and coworkers implemented a co-flow based droplet formation device by inserting a glass pipette into a PDMS device to create a hollow

channel for the continuous phase of flow through [7]. The mechanisms used to convert the droplets formed in the microfluidic device can be classified into heat based [8] [9], light based [10], and chemical reaction based [11] [12]. In addition to microsphere formation with fine control over size, microfluidics has also provided the ability to form non-spherical particles. The length scale of microfluidic devices has been used to confine micrometer-sized droplets into non-spherical shapes and then solidified *in situ*. Doyle group used this technique to synthesize plug and disk shaped particles [13]. Limitations of droplet-based methods are that all the shapes formed are beads or simple deformations of beads and the need to emulsify a droplet before polymerization, which requires optimizing the surface chemistry of the dispersed phase, continuous phase and the device so that the drops can be formed in a continuous and reliable manner.
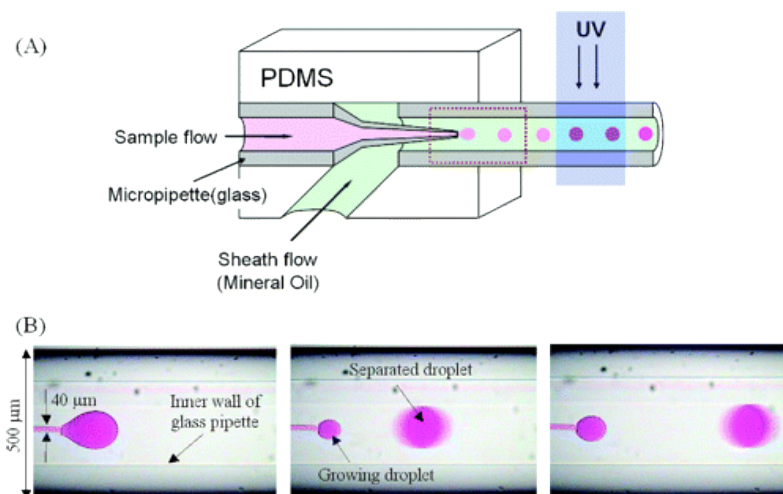
Figure 1.2: Co-flow based droplet formation (a) Schematic illustration of the apparatus used to fabricate microparticles. (b) Snap photographs of the separated microdroplets. Rhodamine B was mixed with the sample fluid for better visualization [7].

To overcome the disadvantages associate with the droplet based methods a new kind of microfluidic methods which use photolithography to define particle shape were developed

by Doyle group [14] [15]. Lithography techniques rely on transparency masks to provide shape definition. Arrays of mask-defined polymeric particles are patterned into a UV light sensitive pre-polymer before being flushed out of the microfluidic device. The ability to create freestanding particles using the flow lithographic method is based on the oxygen inhibition of free radical polymerization reactions at the surface of the PDMS microfluidic device used because oxygen reacts with free radicals to form chain terminating peroxide molecules, resulting in inhibition of polymerization [16]. To address the limitation of resolution at high flow rates in Continuous Flow Lithography (CFL) [14] Stop Flow Lithography (SFL) was developed [15]. In SFL, a flowing stream of pre-polymer is stopped before polymerizing an array of particles into it, providing improved resolution.
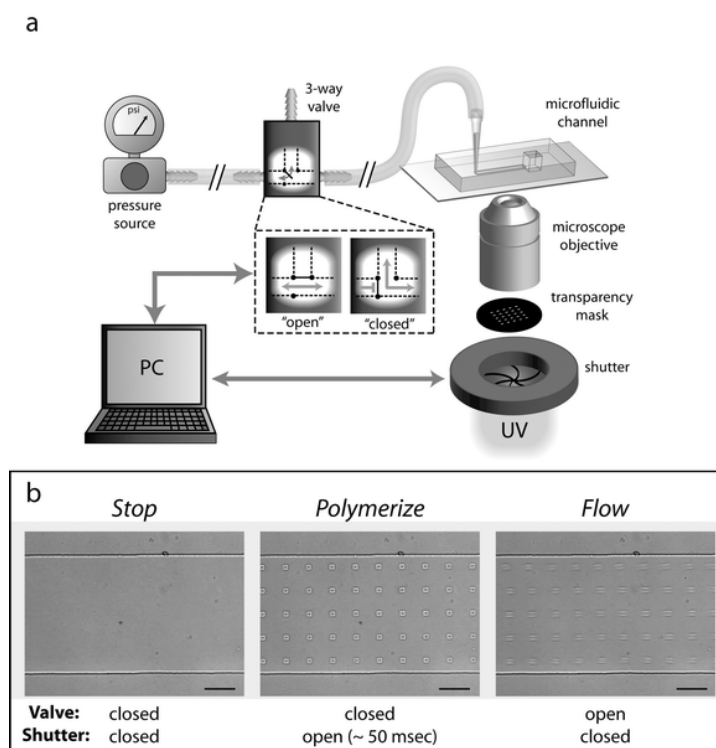
Figure 1.3: (a) Schematic showing the Stop Flow Lithography setup. (b) Microscope images showing the three states of the process [15].
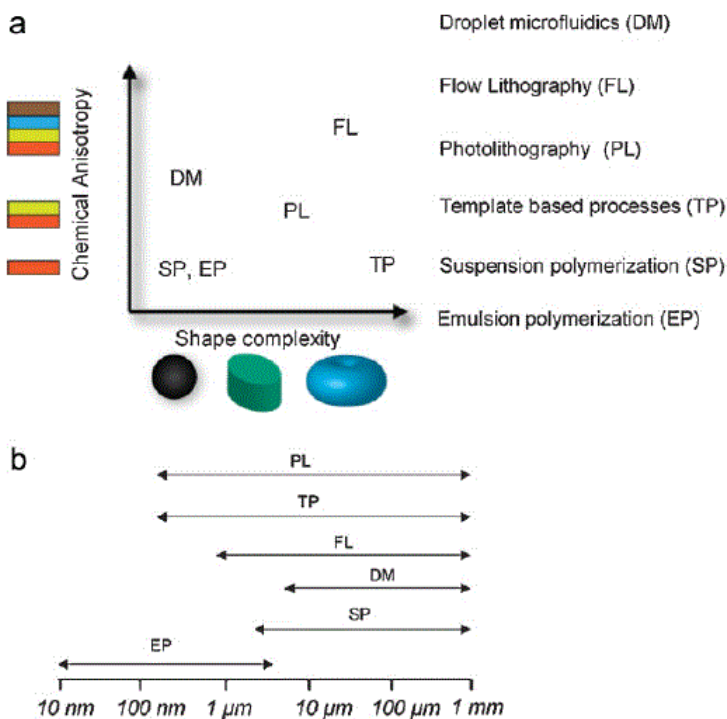
Figure 1.4: a) Different processes extant for particle synthesis classified according to their ability to synthesize complex shapes and multifunctional particles. b) Particle size range covered by the same processes [2].

However, using a physical transparent mask, containing the desired shape for lithography restricts the ability to change the shape on demand. Digital micro-mirror devices (DMD™) can be pre-programmed to change their mask pattern. A Digital micro-mirror device is a rectangular array of several hundred micro-mirrors; these mirrors can be individually tilted to an ON and OFF state. In the ON state, the light is reflected into the lens making those pixels appear bright and in the OFF state, the light is reflected away from the lens making the corresponding pixels appear dark. Kwon group used a DMD device integrated into an optical microscope to synthesize particles with a resolution of 1.54μm x 1.54μm [17] [18].
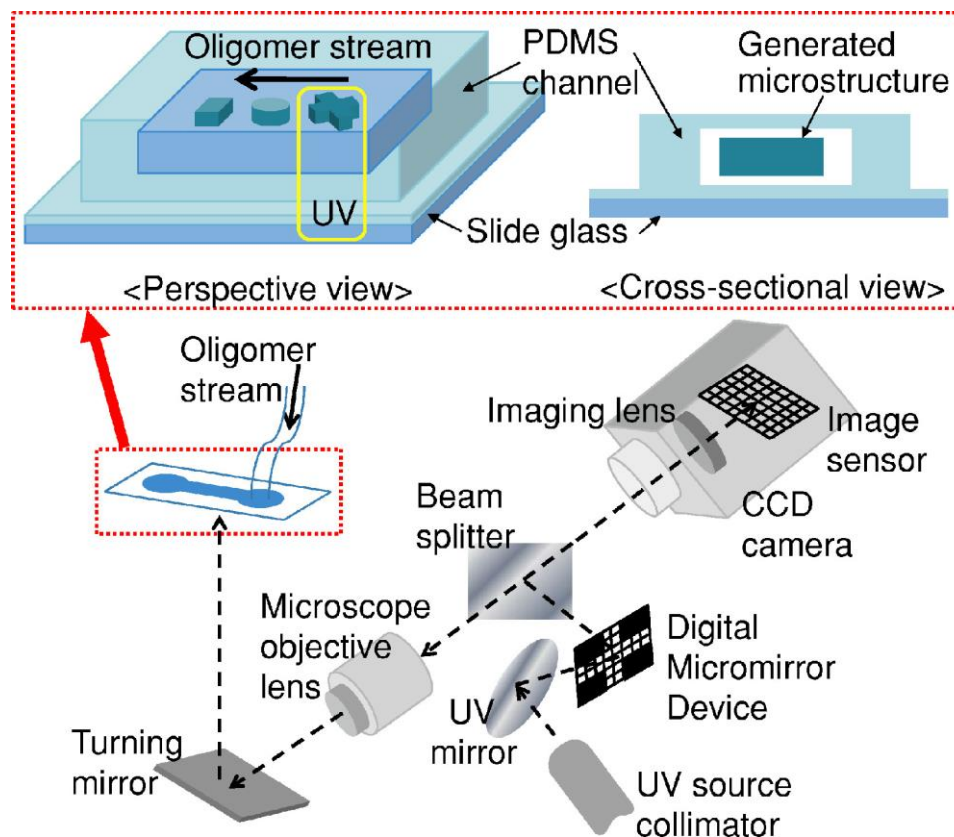
Figure 1.5: Schematic diagram of the optofluidic maskless lithography system for dynamic control of the photopolymerization process in microfluidic devices. [17].

Some of the important applications of complex particle synthesis using microfluidic devices are particle diagnostics and cell and protein encapsulation. Doyle group generated a large number of particles with code patterns. SFL was used to generate particles, one half of which can have any one of the million unique square pattern signatures while the other half contains a probe molecule that is linked to the unique signature [19]. This technique was used to detect DNA oligomers down to the PM level.
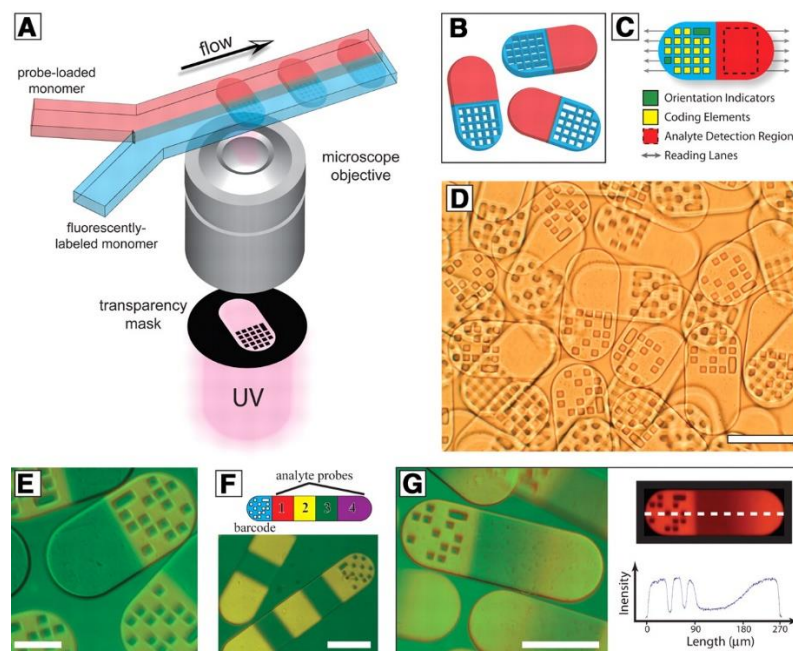
Figure 1.6: Schematic diagram of dot-coded particle synthesis and diagrammatic representation of particle features for encoding and analyte detection. Scale bars indicate 100 μm in (D), (F), and (G) and 50 μm in (E) [19].

Encapsulating cells within hydrogels is also important for generating microenvironment for the cells that native cell architecture and has applications in pharmaceutical research, tissue engineering, personalized drug screening, drug delivery and regenerative medicine. Such micro gels provide 3D microenvironment for living cells allowing individual cells to be independently monitored or manipulated to deliver cells for the repair of damaged tissue [20] [21]. In tissue engineering, cell-containing micro-gels are also used as building blocks that are assembled into larger architectures mimicking the structure of tissues and organs [21]. Takeuchi produced monodisperse droplets containing suspended cells using the technique of water in oil emulsion with the help of a T-junction. They used the internal gelation method to polymerize the particles that involved dispersing an insoluble calcium complex in the Sodium alginate solution. Upon pH reduction, Ca^{2+} ions are released from

the calcium complex, crosslinking the alginate to form a homogenous hydrogel [12]. However, these approaches are not efficient due to the use of continuous oil phase, which significantly decreases the viability of cells due to prolonged exposure to oil and surfactants that are often toxic to cells. To overcome these disadvantages a simple and efficient microfluidic approach to produce monodisperse micro-gels was proposed by utilizing an ultra-thin oil shell of double emulsion drops as a sacrificial template. The cell suspended emulsion drops created are cured by photo polymerization with the help of a UV projection [22]. Even though this method helps reducing the risk of cytotoxicity of the cells due to the exposure to oil and surfactants significantly, it has the limitation of producing only spherical shaped micro-gel particles.
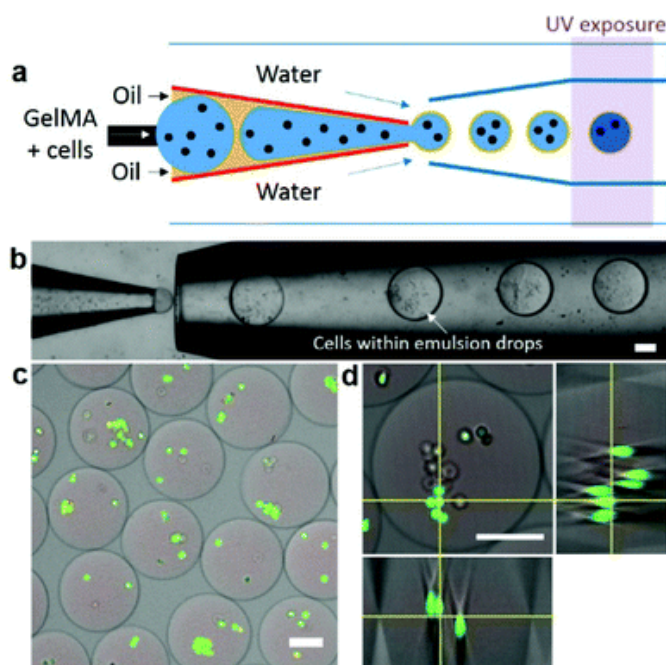
Figure 1.7: (a) Schematic illustration showing the encapsulation of living mammalian cells using the thin-shell double emulsion drops formed with a photo-crosslinkable polymer. (b) Optical image showing cell encapsulation within double emulsion drops. (c) Representative fluorescence microscopy image. (d) Representative fluorescence microscopy image of a single mcirogel containing multiple cells [22].

In order to overcome the limitations of emulsion techniques for encapsulating particles, Doyle group developed a new method to generate cell-laden microgel particles using the idea of stop flow lithography (SFL) [23]. SFL has advantages over emulsion-based techniques in terms of control over size and shape, which plays an important role in drug screening by allowing tagging information to the synthesized micro-particle and in tissue engineering where different shaped micro-particles can be assembled to form larger architectures mimicking structure of tissues or organs. Furthermore, a wide variety of photo-curable material can be used for SFL, facilitating to produce particles of different mechanical, chemical, and biophysical properties.

1.2 Motivation

In all the above-mentioned approaches for particle/cell encapsulation, the particles/cells are randomly suspended in the pre-polymer solution and are encapsulated by various polymerization schemes. Thus, the cured hydrogel particles usually contain multiple particles/cells in a random distribution within the particle. Single cell encapsulation and analysis is highly desired in biological and biomedical engineering because heterogeneous behaviors of genetically identical cells and cell-to-cell variability are of paramount importance for cancer research, developmental biology, drug screening, and stem cell study. In addition, no existing techniques for encapsulating particles/cells has the capability to differentiate different kinds of particles/cells suspended in a single stream of polymer. Therefore capturing a desired cell type in a poly-suspension is still a formidable challenge.

To address this challenge, we propose a new technique for adaptive particle encapsulation with geometrically and biochemically complex micro-particles by combining the state-of-the-art, digital micro-mirror display (DMD^{TM}) and Stop-Flow-Lithography (microfluidics). This combination gives us unprecedented fabrication freedom and capability. The use of micro-fluidics will allow for continuous mass production of micro-particles with various chemical composition and will allow for multi material capability. While the use of digital micro-display optics will allow for dynamic mask generation which will enable one to encode rich information about an individual encapsulated cell such as cell type, lineage, and drug treatment history in each micro-particle. Kwon group used this technique to synthesis particles [17] [18] and encapsulate silicon microchips [24]. By incorporating DMD^{TM} and SFL, we combine the high throughput of SFL and flexibility of the dynamic masked used in PμSL. This powerful technique will offer breakthrough solution for heterogeneity study in proliferation, drug screening, and metastasis at the single-cell level. Furthermore, inclusion of functional species in the micro-particles may potentially lead to directed self-assembly of encapsulated cells.

2 Digital Opto-Fluidic Lithography System Setup

This section will describe the operation and design of the adaptive particle encapsulation system.

2.1 System Description

A UV light source with 405nm light emitting diodes (LED) was purchased from Innovations in Optics (LumiBright, Woburn, MA, USA). The light source is driven by a DC power supply purchased from Agilent Technologies ((E3633A, Santa Clara, CA). The light source was coupled with a digital projector (ASUS B1M LED) which is based on DLP4500® chipset from Texas Instruments (Dallas, TX, USA) consisting of a 0.45" DMD^{TM} with a resolution of 1280 x 800 pixels. A coated wafer stepper objective lens with an effective focal length of 97mm and a magnification of 0.2x was purchased from GCA Tropel (USA) and coupled with the projector. The projection lithography system has a resolution of 3.8 µm/pixel and a light intensity at the focal plane of 29.5 mW/cm^2 when operated with 1 Amp current supply. Maximum light intensity can be upto ~600 mW/cm^2 with a maximum driving current of 20 Amp. Unlike conventional micro-fluidics, where a syringe pump is used to control the flow, here we use a compressed air flow control system [10], which operates on compressed nitrogen. The entire system is controlled using LabVIEW by National Instruments (Austin, TX, USA).
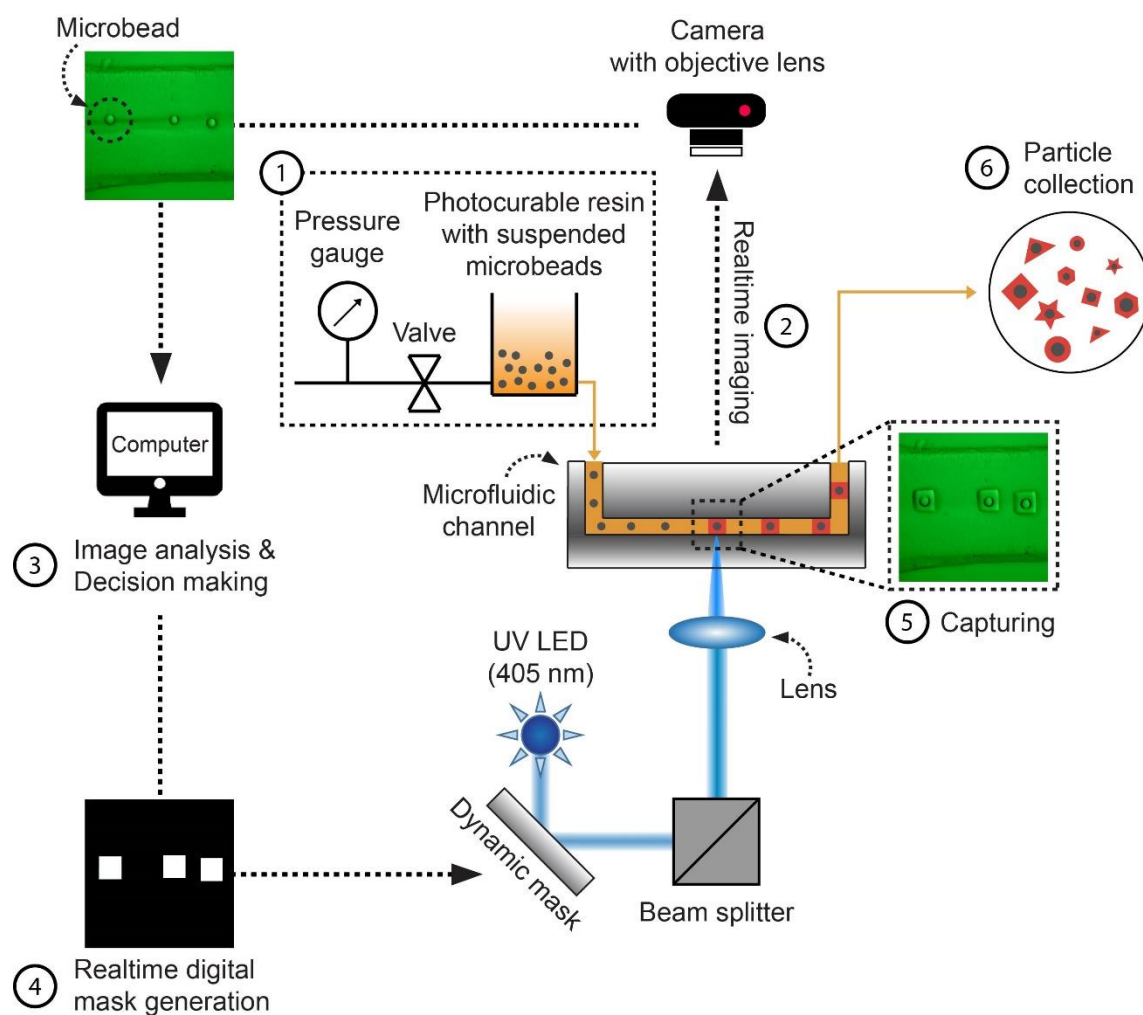
Figure 2.1: Schematic illustration of adaptive particle encapsulation.
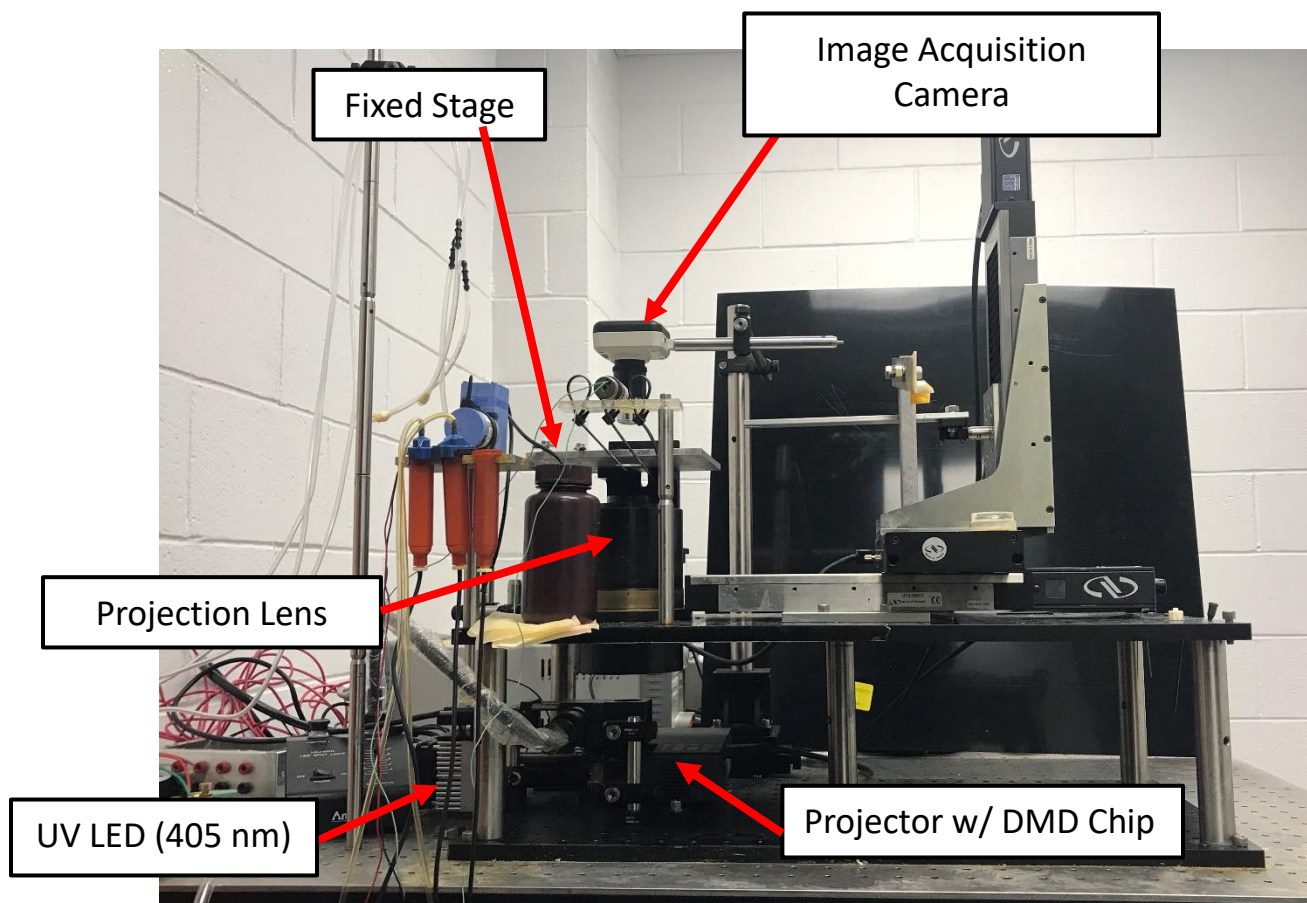
Figure 2.2: Overview of the adaptive particle encapsulation system.

2.2 Programming of the System

The process described in schematic (Figure 2.1) is all contained in the programming of the

LabVIEW (National Instruments, Austin, TX) code. The LabVIEW program combined

with NI-IMAQ driver is able to control the image projection by accessing the UV light

projector as a second monitor for the desktop PC. This allows the program to easily display

the bitmap (BMP) images (Dynamic masks) that will be projected. In order to control the

pressure control system a relay is used which is again controlled by the LabVIEW code. The image processing and dynamic mask generation is done with the help of a MATLAB code. The program flow control of the entire system is shown below in Figure 2.3.
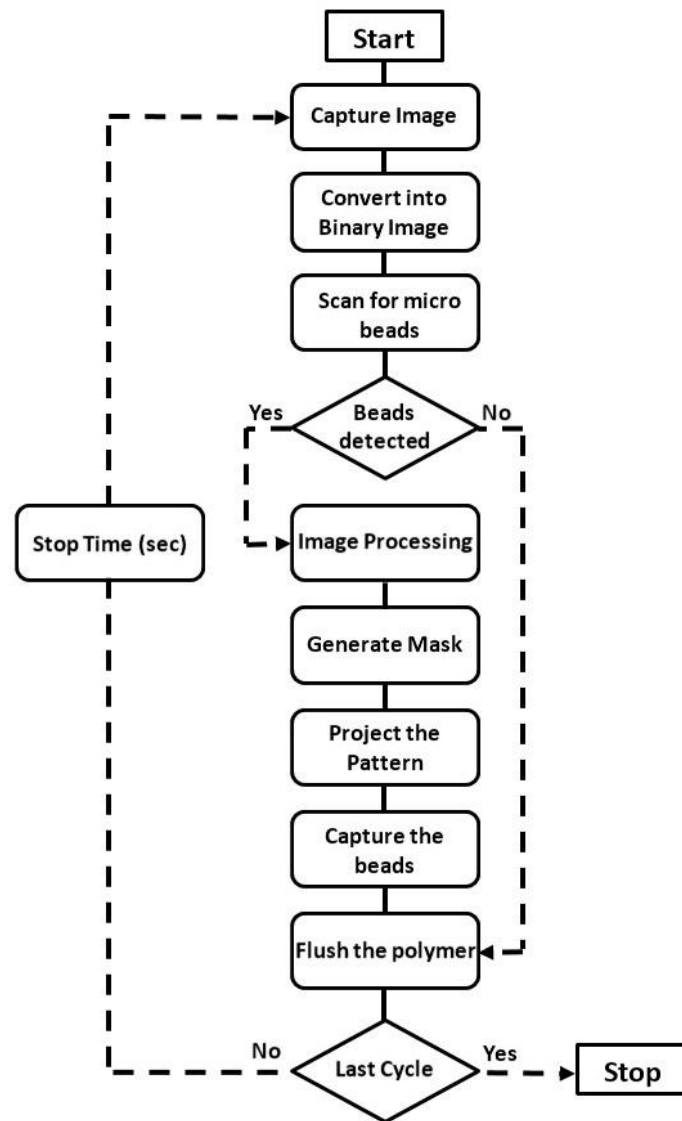
Figure 2.3: Logic of the LabVIEW code.

2.3 Materials

Poly (ethylene glycol) diacrylate (PEGDA, Mw~250) was purchased from Sigma Aldrich (St. Louis, MO, USA). Phenylbis (2,4,6-trimethyl-benzoyl) phosphine oxide which is used as the photo initiator was purchased from Sigma Aldrich (St. Louis, MO, USA). Rhodamine B dye (a pink dye that also fluoresces pink under UV light), and 3,3'-diethyloxacarbocyanine iodide (a yellow dye that fluoresces blue under UV light, referred to as DiOC2) were purchased from Sigma Aldrich (St. Louis, MO, USA). Polystyrene micro beads of various sizes were purchased from Microbeads – Nanobeads (Cold Spring, NY, USA). Ethanol that was used as the solvent for the micro beads was purchased from Decon Labs (King of Prussia, PA, USA). Polydimethylsiloxane (Sylgard 184) was purchased from Dow Corning (Midland, MI, USA). 3-(Trimethoxysilyl) propyl methacrylate was purchased from Sigma Aldrich (St. Louis, MO, USA). (Tridecafluoro-1,1,2,2-Tetrahydrooctyl) Trichlorosilane was purchased from Gelest, INC (Morrisville, PA, USA).

2.4 Polymer Chemistry

Any polymer that can be cured with UV light can be used in this adaptive particle encapsulation system. The polymers used in this thesis is PEGDA 250, which forms the building blocks of the cured resin. In order to make the polymers cure in response to UV light, a photo initiator is added, specifically Phenylbis (2,4,6-trimethylbenzoyl) phosphine oxide. A photo initiator releases free radicals when exposed to the correct wavelength of UV light (405 nm in this case); these free radicals initiate bonding between polymer chains.
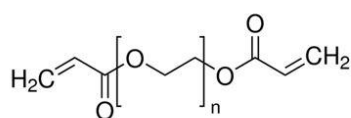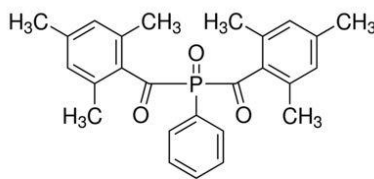
Figure 2.4: Chemical structures of the monomer and photo initiator.
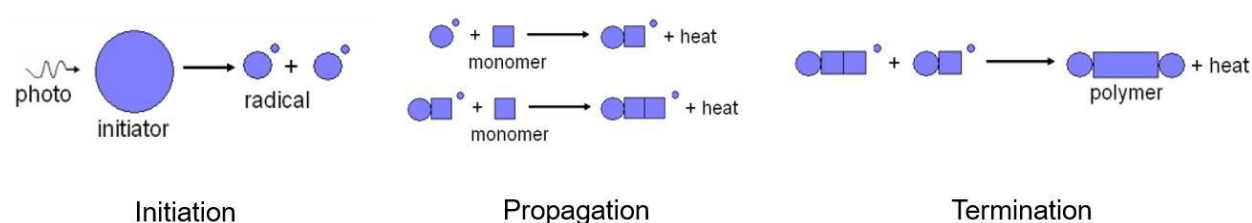
Figure 2.5: Photo polymerization reaction procedure.

Suspended micro bead pre-polymer solution:

One part of 25 mg/ml concentration 40 µm polystyrene micro beads is added to equal amount of ethanol to create a micro bead suspension. Ethanol prevents the agglomeration of the micro beads. This micro bead (MB) suspension is then added to the polymer PEGDA 250 consisting small amounts of photo initiator and stirred on a magnetic stirrer for an hour. The composition used in this thesis is PEGDA 250 + MB 20% v/v + PI 2% wt.
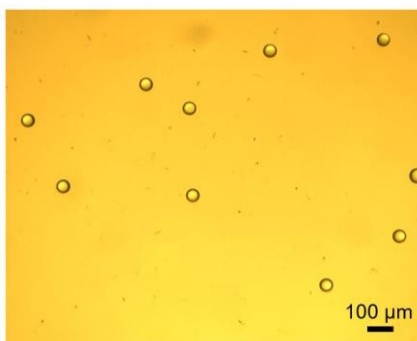
Figure 2.6: Suspended micro bead pre-polymer solution.

2.5 Process

The digital optics based adaptive particle encapsulation system consists of multiple sub systems. The system schematic is shown in Figure 2.1.

First, the pre-polymer resin with suspended micro beads is delivered to the micro-fluidic channel using the compressed air pressure control system with the help of compressed nitrogen. A 3-way valve is used to control the flow of the resin in the micro fluidic channel by turning on and off the air pressure. A 3-way valve helps maintaining the same pressure at both inlet and outlet. Pressure ranging from 1 – 2 psi is applied to drive the pre-polymer resin in the channel. The flow takes a finite time to start and stop because of the deformation of the PDMS due to imposed pressure [9]. The time taken for the flow to stop after the pressure is cut off is called the response time of the flow and the applied pressure of 1~2 psi gives the optimal response time.

Next, the pictures of the suspended particles are taken by a USB camera coupled with a 10x microscopic objective lens. The camera is operated using a LabVIEW module and the images captured are of 1280 x 1024 pixel resolution.

The captured images are then saved on the computer for further processing. The captured images are then analyzed using a MATLAB code for the suspended particles, based on which it generates digital masks to be used for adaptive encapsulation in real-time.

The generated digital image is displayed on the DMD which works as a dynamic mask to modulate a UV light. The UV light is then projected onto the suspended particle in the micro fluidic channel to form a structure and capture the suspended particle. The captured particles are flushed away from the projection site to be collected in the outlet reservoir. This process is repeated for desired number of cycles. Collected particles are transferred to a glass vial and stored in ethanol.

2.6 Microfluidic Device Fabrication

2.6.1 Microfluidic Master Preparation

Unlike traditional SU-8 photoresist lithography process here, we adopt a new method for the fabrication of microfluidic master. The master for the microfluidic device is 3D printed on a glass substrate using PEGDA 250 with 2%wt. of Phenylbis (2,4,6-trimethyl-benzoyl) phosphine oxide as a photo initiator. The glass substrate is coated with 3-(Trimethoxysilyl) propyl methacrylate to promote bonding between cured PEGDA and the glass substrate. In brief, the glass substrate was immersed in 10% Sodium Hydroxide for 45 minutes, rinsed with distilled water and air-dried. The glass slides were then immersed in 3-(Trimethoxysilyl) propyl methacrylate for 15 minutes and incubated overnight in the oven at 70^0C. The incubated slides were then washed with ethanol thoroughly and air-dried before use. A sandwich structure with a treated glass substrate and PDMS film was assembled. The sandwich structure was formed by placing the PDMS film over the coated glass with 150µm spacer plates separating them creating an even space of thickness equal to the spacer plate. This sandwich structure was filled with the pre-polymer solution on

which a UV light modulated by a DMD^{TM} dynamic photomask is projected. The pre-polymer solution undergoes photo-polymerization to form a master on the glass substrate.
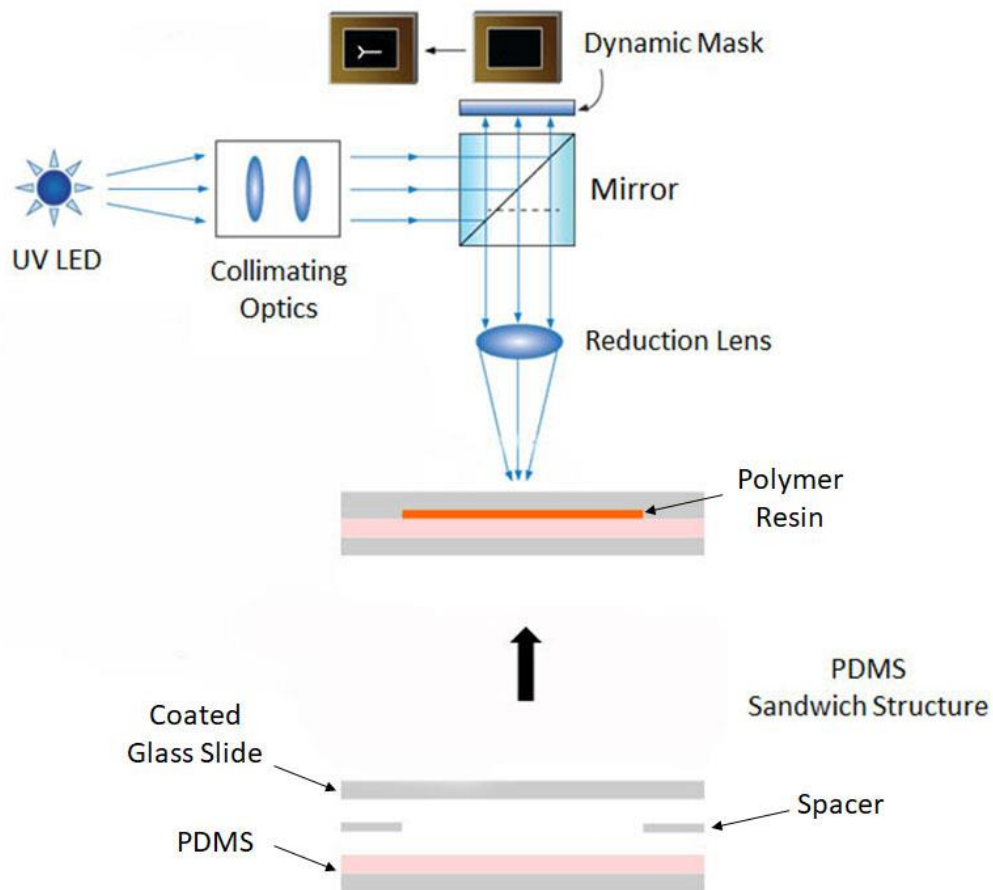
Figure 2.7: Schematic illustration of Microfluidic channel master preparation.

2.6.2 Characterization for Master Preparation

In order to determine the optimal curing time required to fabricate a master with desired width of 500±50 µm and height of 100 – 105 µm a simple study was performed by fabricating different masters by varying the curing time and the obtained results are plotted

in the graph in Figure 2.8. The polymer solution used for the curing test is PEGDA 250 with 2% wt PI. Increase in curing time results in a wider and thicker master.
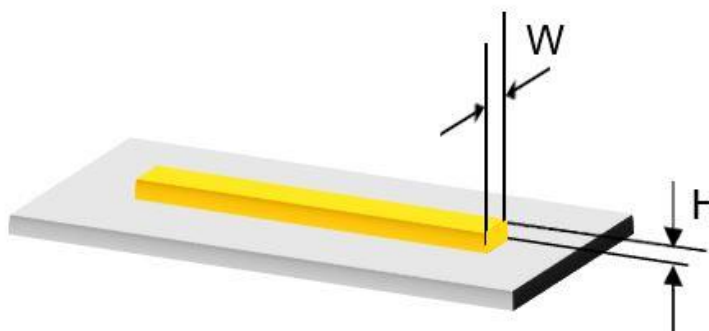
Figure 2.8: Schematic of the microfluidic channel master.
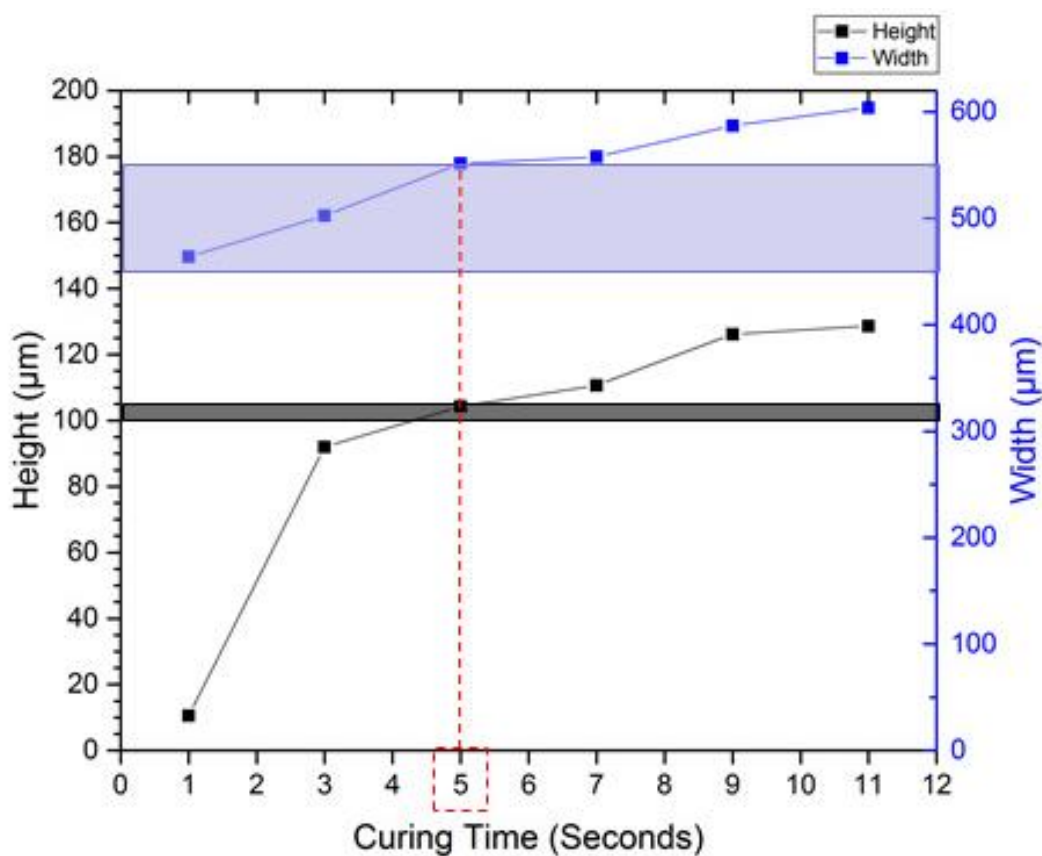
Figure 2.9: Height and Width vs Curing time.Based on the curing test and by analyzing the results from the plot an optimum curing time of 5 seconds was chosen.

2.6.3 PDMS Molding

The glass substrate with the printed micro-fluidic channel master is then coated with (Tridecafluoro-1,1,2,2-Tetrahydrooctyl) Trichlorosilane to help de-molding of PDMS fromt the glass substrate. The base polymer and the curing agent of PDMS are mixed in the weight ratio of 10:1, de-gassed in a vacuum desiccator before pouring it over the 3D printed microfluidic master. The PDMS is cured in the oven at 70^0C for 4 hours to form the microfluidic device. The microfluidic device was then bonded to a cured flat PDMS substrate to make a complete micro fluidic channel device.
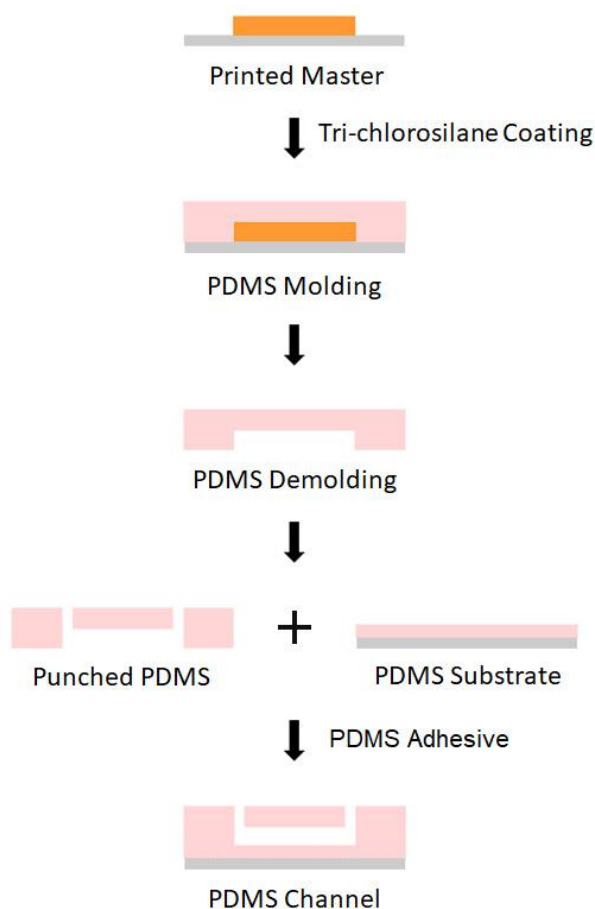
Figure 2.10: Schematic illustration of PDMS Microfluidic channel molding.

Figure 2.11: Fabricated PDMS Microfluidic channels. Scale bars 5 mm.

2.7 Pressure Control System

Unlike conventional micro-fluidics, where a syringe pump is used to control the flow, here we use a compressed air flow control system [25]. Syringe pumps provide volumetric flow that does not have a rapid dynamic response, while a pressure driven flow has a very rapid dynamic response and the volumetric flow can merely be controlled by controlling the pressure. The pressure control system is as shown in the Figure 2.7, the compressed air is connected to an omega pressure regulator which was then connected to a three-way solenoid valve (Model U8356A002V, ASCO Valves, NJ, USA) with one outlet left as a vent to the atmosphere and the other connected to the pressure distribution manifold. The three-way valve helps maintaining atmospheric pressure at inlet and outlet when closed, which aids in maintaining a fluctuation free flow. A series of control channels were branched off the main supply line, each with its own needle valve for venting. In addition, a pipette tip (ART 200, Thermo scientific) was inserted in each branch to increase resistance and provide more even pressure to all the control channels. If the needle valves are all closed the pressure in all the control branches are same and as the needle valves are opened, the pressure in the respective branch drops, lowering the flow rate of the resin. The pressure gauge on each branch shows the individual pressure for the branch.

This pressure control system can further be used for fluid stream focusing in a multi inlet microfluidic channel by individually changing the pressures in the branches. Figure 2.9 shows fluid stream focusing in a 3 inlet microfluidic channel.
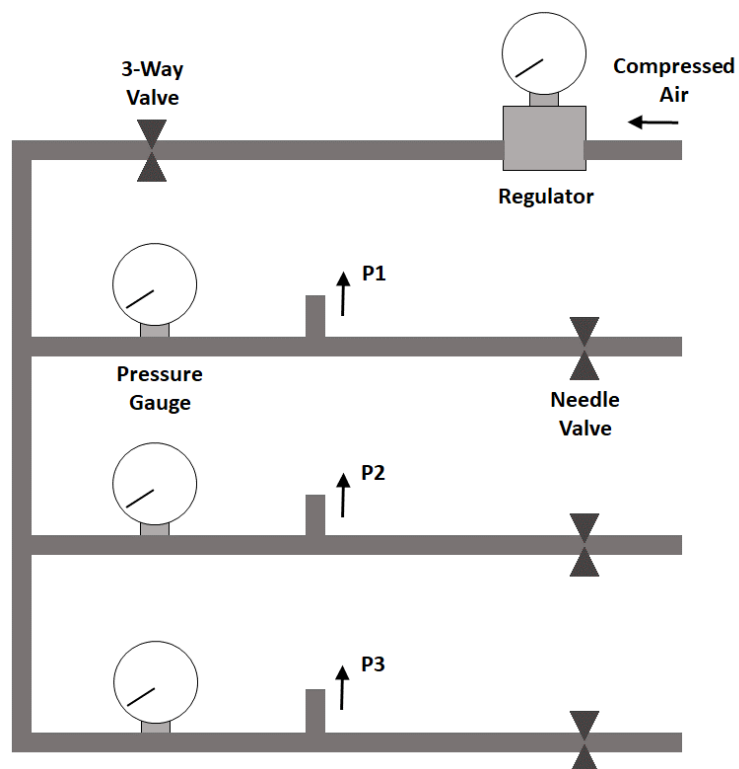
Figure 2.12: Schematic of the pressure control system.
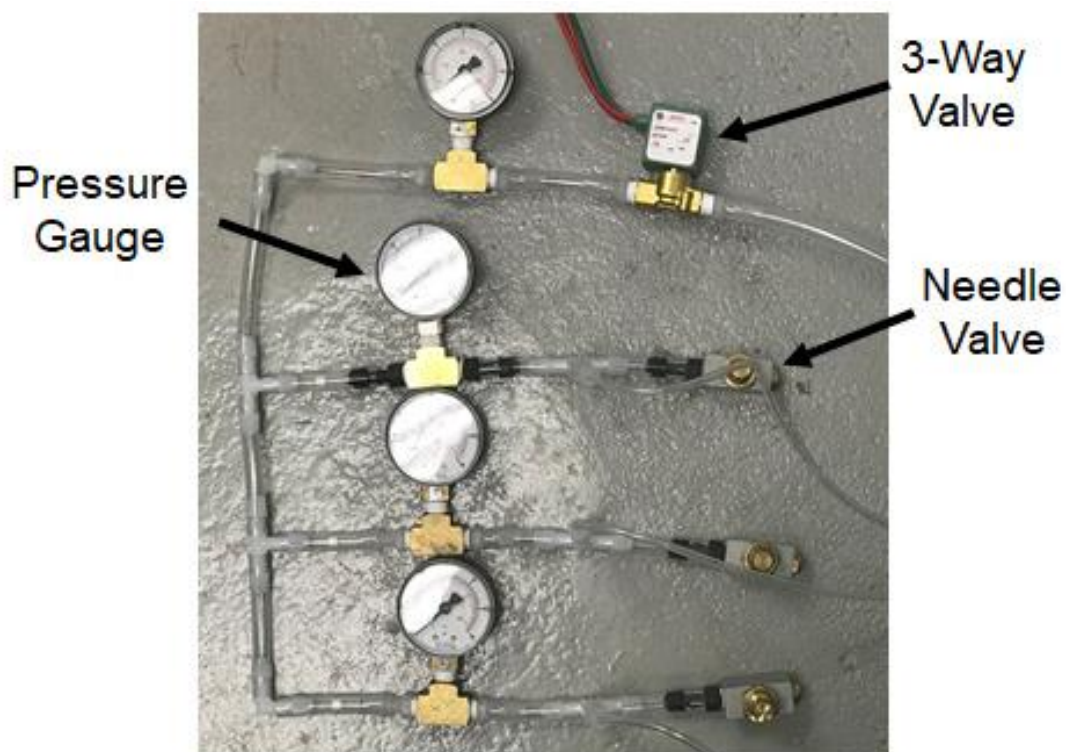
Figure 2.13: Photo of the pressure control system.
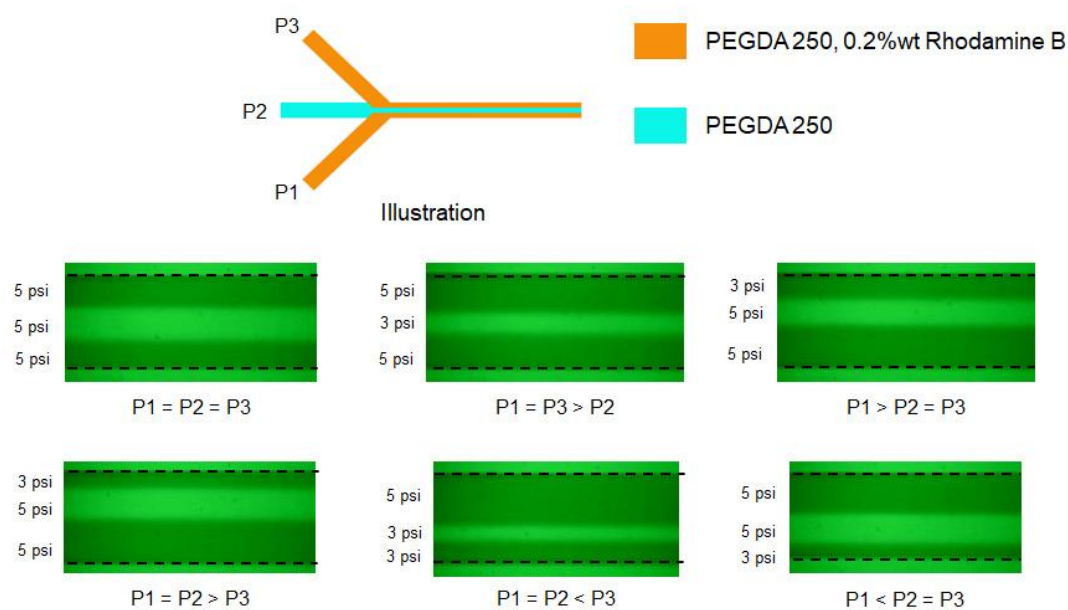
Figure 2.14: Fluid stream focusing in a 3-inlet Microfluidic channel.

2.8 Image/Video Acquisition System

The image/Video capturing system consists of a USB camera Moticam 1SP from Motic®
(China) coupled with a 10X objective lens and a 6 Watt LED spot light source from
AmScope. The white light from the LED is filtered using a bandpass filter, which has a
center wavelength of 532nm and a bandwidth of 10nm (FLH532-10, Thorlabs). The whole
system acts like an inverted microscope in transmission mode.

The light from the LED has to be filtered using a bandpass filter to prevent photo-
polymerization of the pre-polymer in the channel as the polymerization is triggered when
light in the wavelength range of 365~405nm is incident on it. The USB camera is connected
to a computer and is operated by using the software Motic Image plus 2.0 provided by the
manufacturer to capture images and videos.

3 Adaptive Particle Encapsulation

3.1 Curing Test

In order to determine the smallest particle dimension resolvable with the current system a curing test was performed by printing a slotted rectangle of different dimensions. The conditions maintained during the test were slightly different from that of a microfluidic channel. In a microfluidic channel the printed structures are surrounded by PDMS on all four sides enabling them to advect through the flowing polymer solution. This is because of the oxygen induced-inhibition of polymerization at the PDMS surface [26], which in the present case makes is very tedious to retrieve the printed structure for examination. Hence the structures were printed in a sandwich structure consisting of a coated glass slide and a PDMS film. The sandwich structure was assembled by placing the PDMS film under the coated glass with 150µm spacer plates separating them creating an even space of thickness equal to the spacer plate. This sandwich structure was filled with the pre-polymer solution on which a UV light modulated by a DMD^{TM} dynamic photomask is projected. The quality of the printed structure depends on the curing time and the size of the structure. Hence pre-polymer solutions containing 2%wt of Phenylbis (2,4,6- trimethyl-benzoyl) phosphine oxide was tested by printing structures of different sizes with different curing times. Based on the results the smallest structure printable with acceptable resolution is around 240 x 240µm. By investigating the microscopic images of the printed structures and comparing the dimensions of the structures it is observed that a micro-fluidic channel of 500µm width and pre-polymer solution of 2% weight concentration of Phenylbis (2,4,6- trimethyl-benzoyl) phosphine oxide with curing time of 2 seconds are the optimal conditions.
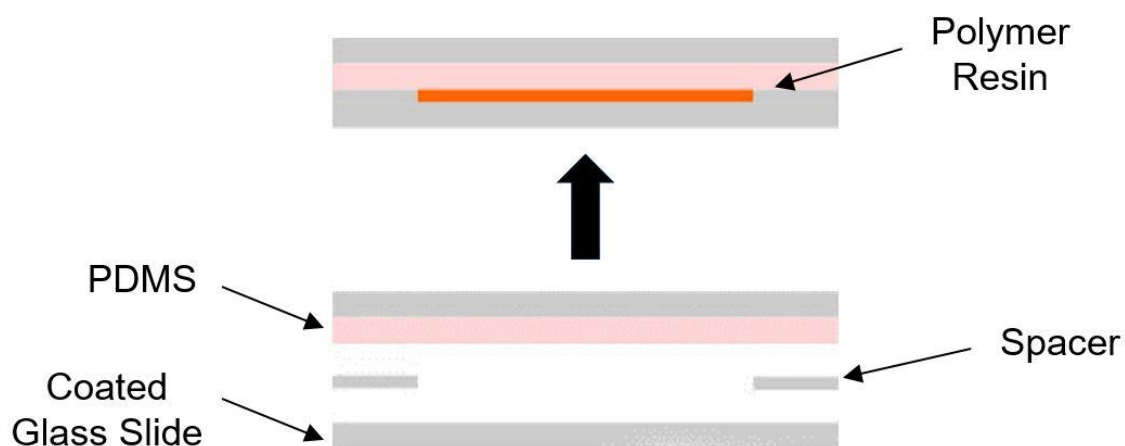
Figure 3.1: Schematic of a PDMS sandwich structure.

Monomer	PI (%wt)	Curing time (s)
PEGDA 250	2	1
		1.5
		2
		2.5
		3

Table 3.1: Curing test experimental parameters.
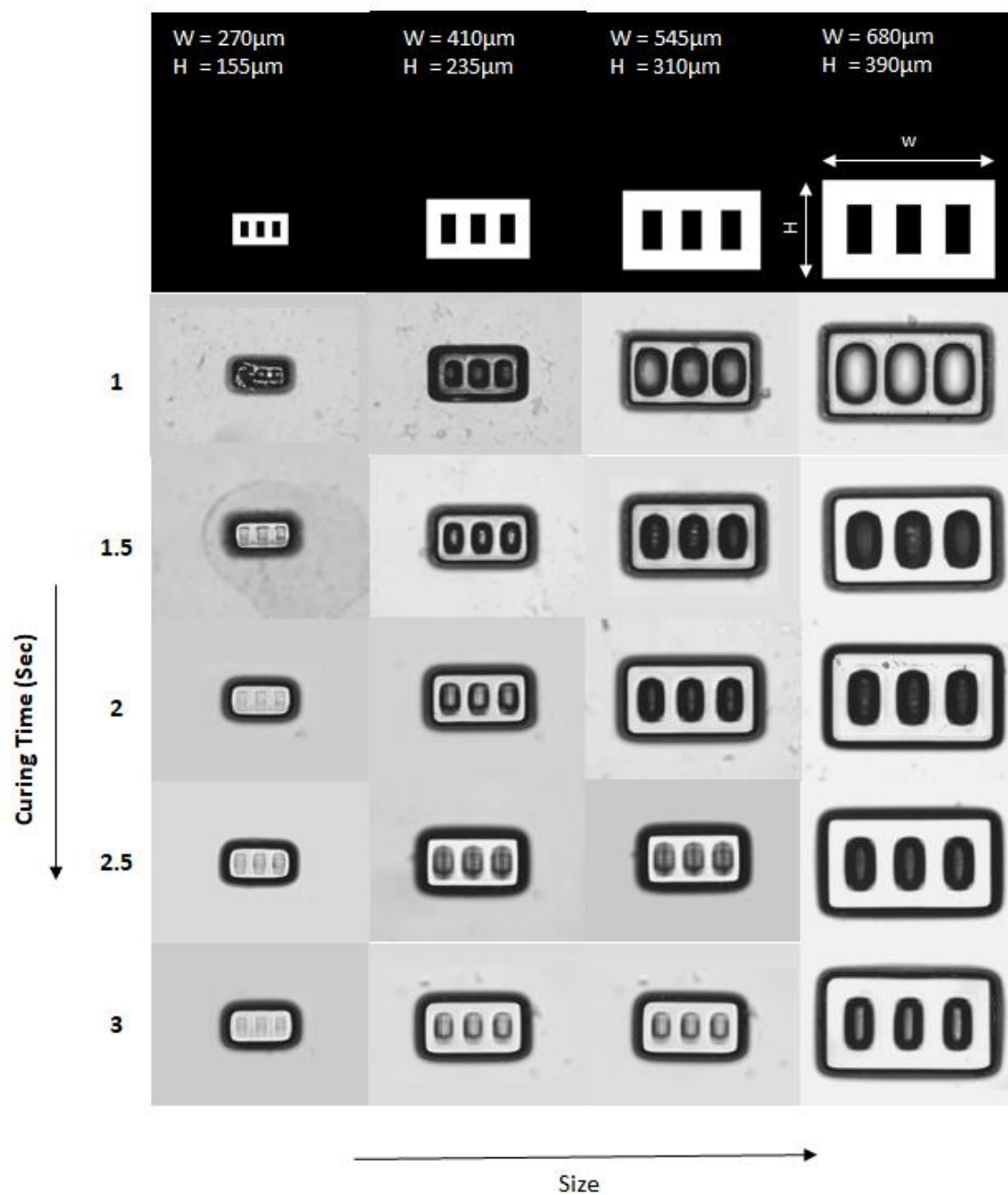
Figure 3.2: Curing time vs size plot for pre polymer resin with 2 wt% PI.
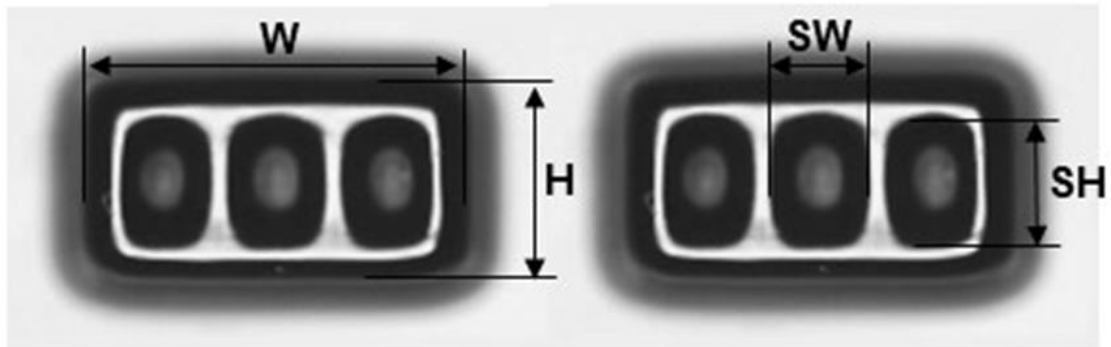
Figure 3.3: Curing test particle measurement scheme.

	Width (µm)	Height (µm)	Slot Width (µm)	Slot Height (µm)
Expected Dimensions	410	235	57	114
1 Sec	377±1.8	214±0.4	72±7.5	108±4.2
1.5 Sec	382±1.6	221±1.2	80±3.9	116±1.3
2 Sec	401±1.3	229±1.3	78±1.7	118±0.8
2.5 Sec	414±0.3	231±1.7	79±2.1	123±1.7
3 Sec	416±2.8	229±2.5	71±0.9	125±1.5

Table 3.2: Curing time study results.

3.2 Micro-Particle Synthesis

Photocurable pre-polymer solution is introduced to a transparent PDMS microfluidic channel using a compressed air based pressure control system. A pressure of 1~2 psi was used. When the flow is stopped, an image containing desired patterns is projected using the digital dynamic mask on to the pre-polymer solution in the microfluidic channel, forming micro-particles by photo-polymerization. The BMP images of 1280 x 800 pixel resolution were created using Adobe Photoshop (San Jose, CA, USA). The response time for the flow of the pre-polymer to stop when the pressure is cut off was 0.5 second, which is very quick compared to the conventional technique of using a syringe pump. The time required for photo polymerization to occur to form particles of the desired shape and accuracy was 1 second with the LED source operated with an intensity of 59 mW/cm^2 at the focal plane. The printed micro particles were flushed away from the fabrication site and were allowed to be collected in a pipette tip at the outlet of the micro fluidic channel. This stop-flow-lithography (SFL) cycle is repeated until the required number of particles were fabricated. The printed particles were transferred from the pipette tube to a glass viale and were stored in ethanol. The collected particles were transferred to a glass petri dish as required using a pipette tip for microscopic images.

3.2.1 Basic Stop Flow Lithography

Single Material:

In order to test the basic SFL capability using the curing characteristics and parameters we determined in the curing test described above, we printed triangular and circular shaped particles. The particles shown in Figure 3.4 were printed using the technique of

conventional SFL except that a digital mask was used to pattern UV instead of a physical mask.

The particles were printed in a 100µm deep and 500µm wide micro fluidic channel using a pre-polymer solution. The cycle time to print the particles was 3.5 seconds, consisting of 1 second of flow time, 0.5 seconds of a stop time and, 2 seconds of an exposure time. Flow time is the time needed to flush away the printed particles from the polymerization site, stop time is the time taken by the flow to stop once the pressure is cut off, and exposure time is the time required for the photo-polymerization to take place and produce structures of desired dimensions. The production rate of particles is ~3100 particles/hour with three particles printed per cycle.

Printed particles were collected after 800 ~ 900 cycles and optical and scanning electron microscope (SEM) images were taken (Figure 7). The circular particles with an expected diameter of 190 um turned out to have an average diameter of 197 microns with a standard deviation of 4.8 microns. While the triangular particles were expected to have 60^0 angle, the printed particles turned out to have an average angle of 58.62^0 with a standard deviation of 4.6^0.
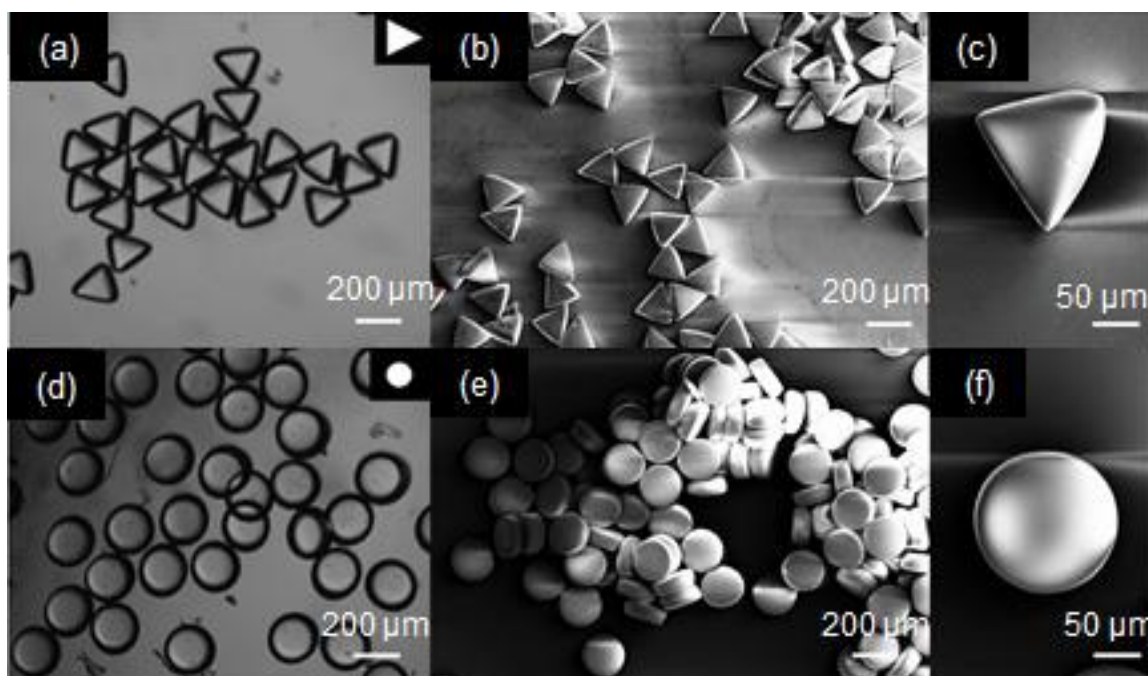
Figure 3.4: Particles printed via Stop-Flow Lithography: images (a) (d) are optical microscopy images, (b) (c) (e) (f) SEM images. Scale bars 200µm (a) (b) (d) (e) & 50µm (c)(f).
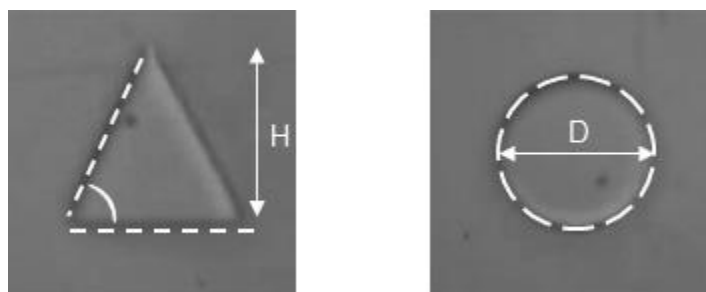
Figure 3.5: Triangular and Circular particle measurement scheme.

	Angle	Height (µm)
Expected	60^0	190
Measured	58.6 ± 4.6^0	195.1 ± 4.2
% Error	7.2	2.9

Table 3.3: Triangular particle dimensional analysis.

	Diameter (μm)
Expected	190
Measured	197.3±4.8
% Error	3.9

Table 3.4: Circular particle dimensional analysis.

Multi Material:

In order to demonstrate the multi material capability of SFL we printed rectangular particles. The particles shown in Figure 3.6 were printed using the technique of conventional SFL using a digital mask in a 2 inlet microfluidic channel utilizing the concept of fluid stream focusing.

The particles were printed in a 100μm deep and 500μm wide micro fluidic channel using a pre-polymer solution 1 consisting of Poly (ethylene glycol) diacrylate Mn250 with 2% by weight Phenylbis (2,4,6- trimethyl-benzoyl) phosphine oxide. Pre-polymer solution 2 consisting of Poly (ethylene glycol) diacrylate Mn250 with 2% by weight Phenylbis (2,4,6- trimethyl-benzoyl) phosphine oxide and 0.01% wt Rhodamine B was used as the second material. The pressure control system was operated at 2PSI to drive the flow in the micro fluidic channel and the current used for the UV LED was 4amp, which produces a maximum intensity of 118 mW/cm^2.

The cycle time to print the particles was 2 seconds. The cycle time includes 1 second of flow time, a stop time of 0.5 seconds and a curing time of 0.5 seconds. The printed squares

which were expected to have an edge length of 190 microns turned out to be having an average edge length of 188.3 microns with a standard deviation of 6.03 microns (n=25).
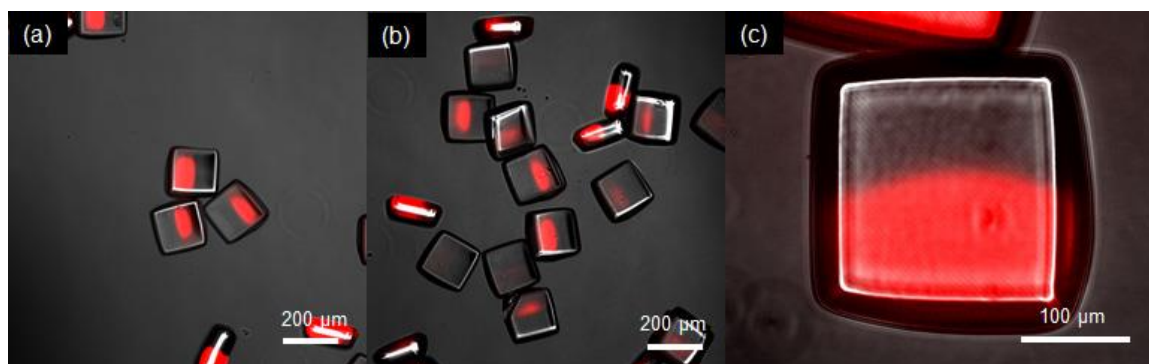
Figure 3.6: Fluorescence microscope images of particles printed via Multi-material SFL. Scale bars 200µm (a) (b) & 100µm (c).

Figure 3.7: Multi-material particle measurement scheme.

	Edge (µm)
Expected	190
Measured	188.39±6.03
% Error	4.6

Table 3.5: Multi-material particle dimensional analysis.

3.2.2 Dynamic Stop Flow Lithography

Single Material:

In order to demonstrate the capability and advantages of a digital dynamic mask, we printed particles with alphabets and numbers. By digitally changing the mask for each projection, different particles can be printed in each cycle without the need for stopping the SFL process for mask change and alignment. This capability of changing the mask dynamically on demand is one of the advantages of a dynamic mask over the conventional physical mask based stop flow lithography.
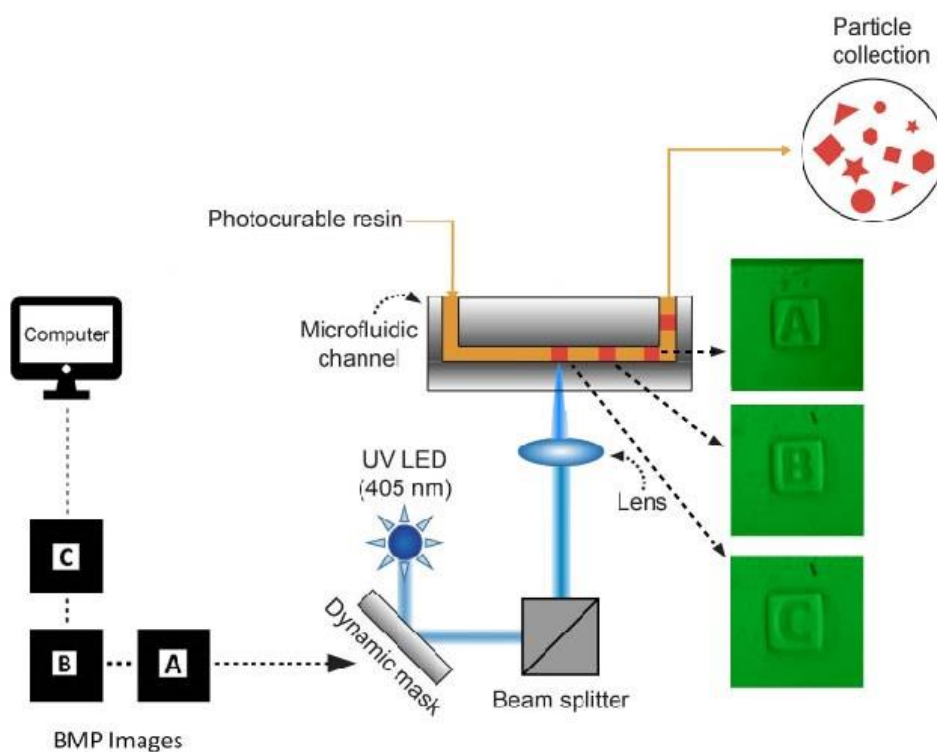
Figure 3.8: Schematic of Dynamic SFL.

The particles shown in Figure 3.9 were printed in a 100µm deep and 500µm wide micro fluidic channel using a pre-polymer solution consisting of Poly (ethylene glycol) diacrylate Mn250 with 2% by weight Phenylbis (2,4,6- trimethyl-benzoyl) phosphine oxide. The

pressure control system was operated at 1PSI to drive the flow in the micro fluidic channel and the current used for the UV LED was 2amp, which produces a maximum intensity of 59 mW/cm^2.

The cycle time to print the particles was 3.5 seconds. The cycle time includes 1 second of flow time, a stop time of 0.5 seconds and a curing time of 2 seconds. The printed alphabets which were expected to have an edge length of 190 microns turned out to be having an average edge length of 203 microns with a standard deviation of 4.4 microns (n=25). While the printed numbers were expected to have an edge length of 190 microns turned out to be having an average edge length of 200 microns with a standard deviation of 4.6 microns (n=25).
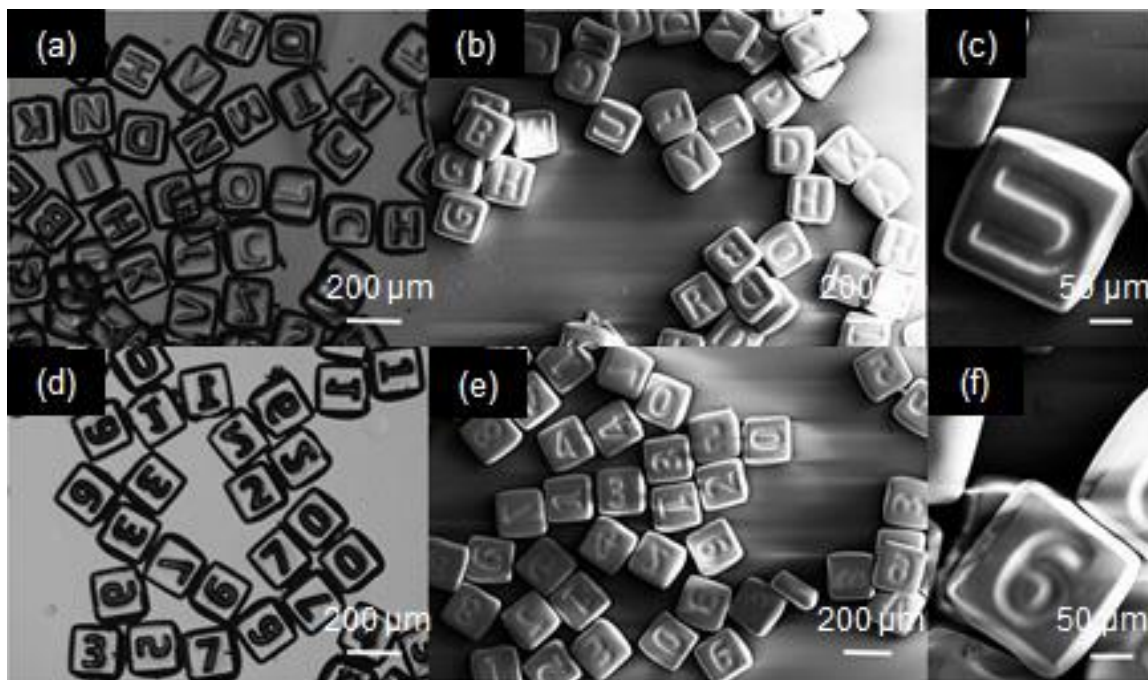

Figure 3.9: Particles printed via Dynamic Stop-Flow Lithography: images (a) (d) are optical microscopy images, (b) (c) (e) (f) SEM images. Scale bars 200µm (a) (b) (d) (e) & 50µm (c)(f).
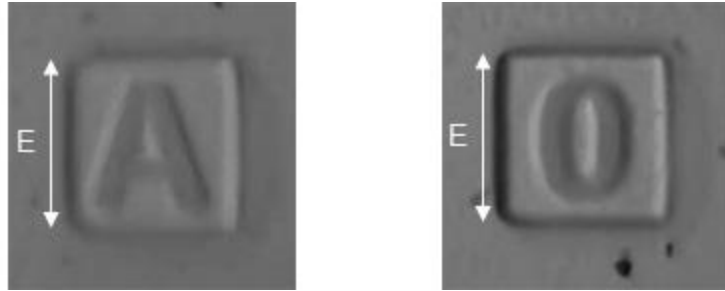
Figure 3.10: Alphabets and Numbers particle measurement scheme.

	Edge (μm)
Expected	190
Measured	203±4.4
% Error	1.6

Table 3.6: Alphabets particle dimensional analysis.

	Edge (μm)
Expected	190
Measured	200±4.6
% Error	0.4

Table 3.7: Numbers particle dimensional analysis.

Multi Material:

In order to demonstrate the multi material capability of Dynamic SFL we printed rectangular particles. The particles shown in Figure 3.11 were printed using the technique of SFL using a digital mask in a 2 inlet microfluidic channel utilizing the concept of fluid stream focusing.

The particles were printed in a 100µm deep and 1000µm wide micro fluidic channel using a pre-polymer solution 1 consisting of Poly (ethylene glycol) diacrylate Mn250 with 2% by weight Phenylbis (2,4,6- trimethyl-benzoyl) phosphine oxide and 0.01% wt $DioC_2$. Pre-polymer solution 2 consisting of Poly (ethylene glycol) diacrylate Mn250 with 2% by weight Phenylbis (2,4,6- trimethyl-benzoyl) phosphine oxide and 0.01% wt Rhodamine B was used as the second material. The pressure control system was operated at 2PSI to drive the flow in the micro fluidic channel and the current used for the UV LED was 4amp, which produces a maximum intensity of 118 mW/cm^2.

The cycle time to print the particles was 2 seconds. The cycle time includes 1 second of flow time, a stop time of 0.5 seconds and a curing time of 0.5 seconds. The printed squares which were expected to have an height of 400 microns turned out to be having an average edge length of 387.2 microns with a standard deviation of 11.01 microns (n=25) and width of 455 microns turned out to be having an average edge length of 444.1 microns with a standard deviation of 14.05 microns (n=25).
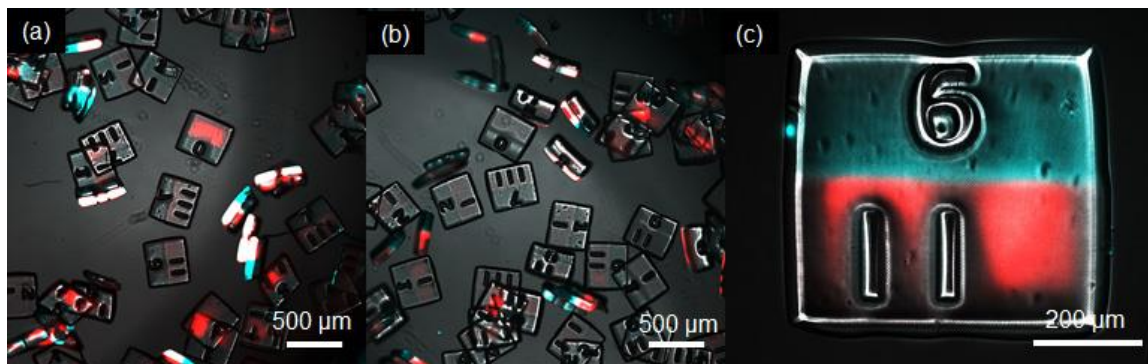
Figure 3.11: Fluorescence microscope images of particles printed via Multi-material Dynamic SFL. Scale bars 500µm (a) (b) & 200µm (c).
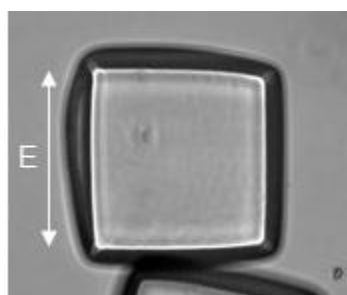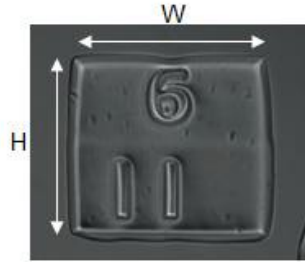
Figure 3.12: Binary multi-material particle measurement scheme.

	Height (µm)	**Width (µm)**
Expected	400	455
Measured	387.2±11.1	444.1±14.5
% Error	3.5	2.8

Table 3.8: Binary multi-material particle dimensional analysis.

3.3 Adaptive Stop Flow Lithography

A digitally reconfigurable dynamic photomask for lithography allows for real-time generation of photomasks based on the information acquired from the microfluidic channel. In our case, when a micro particle suspended pre-polymer resin flows into a micro fluidic channel, visual information of the suspended particles such as shape, size, and location is acquired using a digital camera. This information is processed to generate encapsulation patterns, which are then sent to the DMD^{TM} to produce the projection UV light. The UV light projected onto the micro particles with desired patterns causes the surrounding pre-polymer to polymerize, encapsulating the micro-particles possibly with geometrically encoded patterns. The above process is repeated for multiple cycles for massive and adapted encapsulation.

3.3.1 Scaling, Offset, and Rotation

In order to perform adaptive encapsulation of the particles one on one mapping of the pixels

of the captured images by the camera (1280X1024) to those of the DMD^{TM} (1280X800) is

required. A detailed procedure with process steps is shown in Figure 3.17.

First, a braille grid in is printed as a calibration pattern. The pattern is designed such that

there is no rotational symmetry. The printed pattern is placed on the focal plane and its

image is captured using the image acquisition camera (step 1). The captured image of

resolution 1280 x 1024 is then converted into a binary image based on threshold using the

function "imbinarize" (step 2). The "imbinarize" function creates a binary image from the

input image by replacing all values above a globally determined threshold with 1's and

settling all other values to 0's. Threshold specifies a scalar luminance value or a matrix of

luminance values; threshold must have a value between 0 and 1. The binary image is

inverted and noise from the surroundings or light is filtered out in the next step (step 3).

The inverted image is then used to detect the coordinates and radius of the circles using the

"imfindcircles" function from the MATLAB image-processing library, which is based on

the Circular Hough Transform (CHT) algorithm for finding circles in an image.

Step 1: Captured Image
(1280x1024)

Step 2: Binary Image
(1280x1024)

Step 3: Reduced noise inverted Image
(1280x1024)
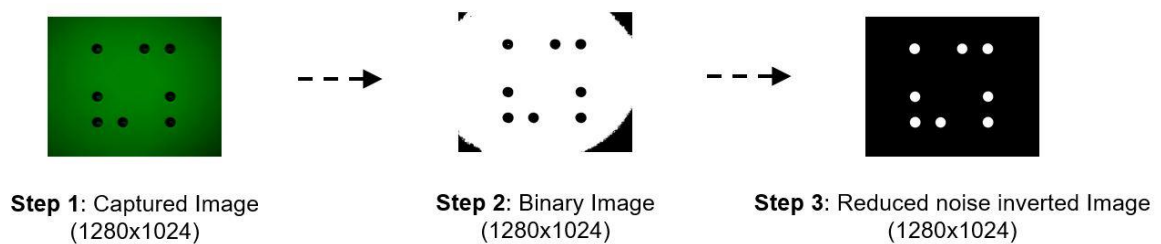
Figure 3.13: Image binarization and inversion.

The next step is to match the resolution of the captured image and that of the DMD^{TM}. For that, the initial BMP image used to print the grid is compared to that of the image in step 3 and a resize factor is determined. The resize factor is determined as a ratio of the distance between the circles from the image in step 3 to that of the initial BMP image used to print the braille grid. The determined resize factor is then applied to the reduced noise image to convert it into a lower resolution image. After resizing the reduced resolution image is used to determine a new set of center coordinates and radii of the circle. The newly determined coordinates and radii are then used to plot circles on a 1280 x 800 black background image. Radii of the circles are modified by applying a scaling factor (step 4). Scaling factor is determined by comparing the radii of the circles on the image in step 3 to that of the circles on the initial BMP image used to print the grid, this is done to match the dimensions of the circles.

Step 3: Reduced noise inverted Image
(1280x1024)

Step 4: Scaled Image
(1280x800)
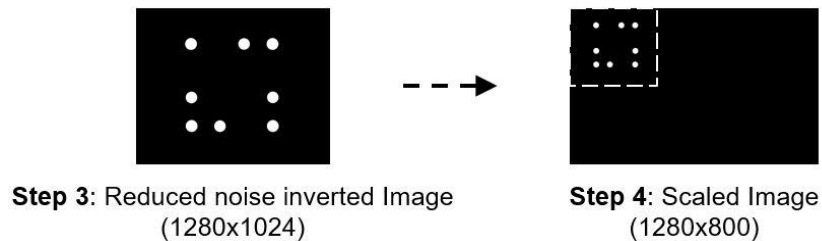
Figure 3.14: Image scaling.

The next step is to translate the circles to match them with the original BMP (step 5), for this X and Y translation factors are determined simply by measuring the distance between the centers of the circles on the image in step 4 and the centers of the circles on the initial BMP image.

Step 4: Scaled Image
(1280x800)

Step 5: After Translation
(1280x800)
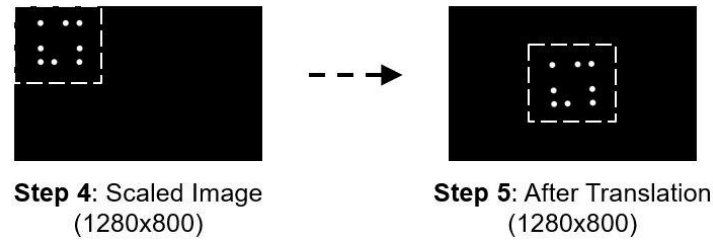
Figure 3.15: Pixel translation.

Step 5: Translated Image
(1280x800)

Step 6: After Rotation
(1280x800)
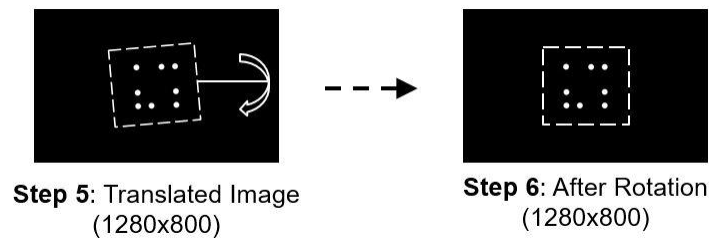
Figure 3.16: Image rotation.

Finally, the image is rotated by a small angle until any rotational miss-match is corrected (step 6). The rotation angle is determined by trial and error comparing the image in step 5 to the initial BMP image. The resize factor, scaling factor, translation factors and rotational angle are recorded, which are later used while encapsulating the particles in a micro fluidic channel.

Figure 3.18 shows the initial BMP image used to print the braille grid, the dynamically generated BMP by image processing and an overlay of both the images to display the accuracy. The misalignment is about 12 µm (~3 Pixels).

(a) **Step 1**: Acquired Image
(1280 x 1024)

(b) **Step 2**: Image
Binarization

(c) **Step 3**: Image inversion
and noise reduction

(d) **Step 4**: Applying scaling factor
(1280 x 800)

(e) **Step 5**: Translation of
the pixels

(f) **Step 6**: Final mask after
rotation
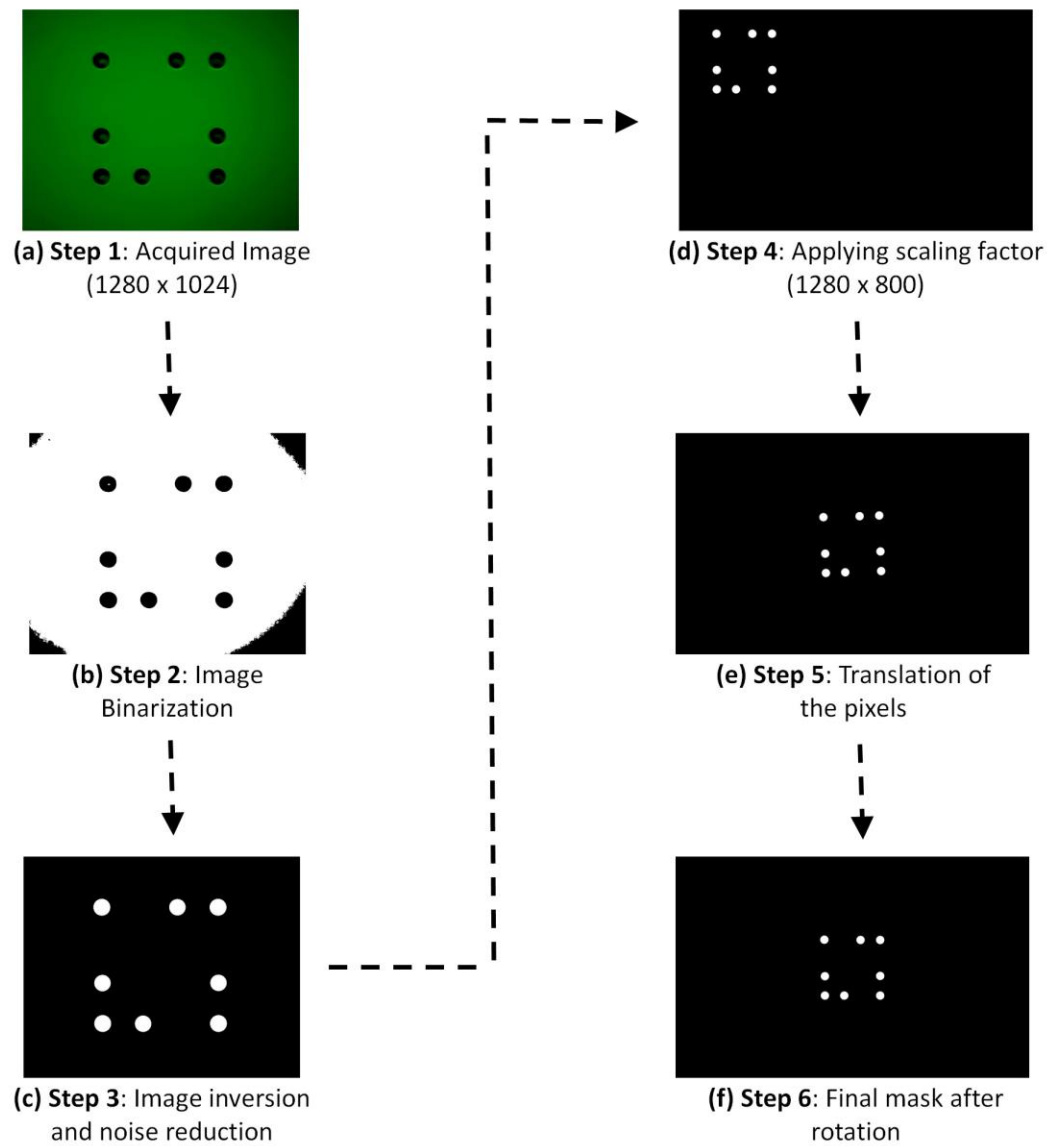
Figure 3.17: Process steps for pixel-to-pixel mapping of the captured image and DMD^{TM}.
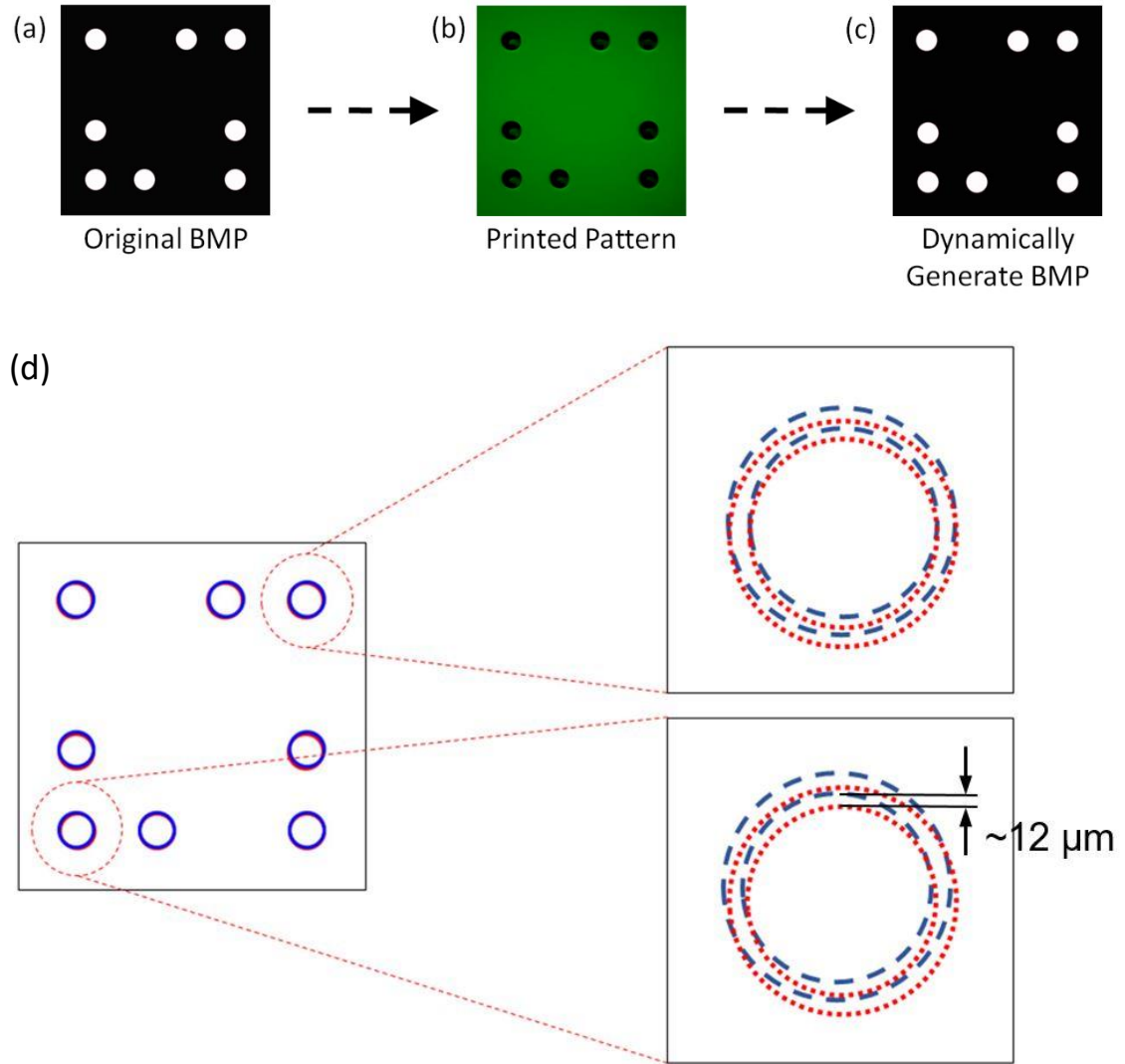
Figure 3.18: Original mask vs Dynamically generated mask (a) the BMP image used to print the braille grid.(b) captured image of the braille grid (c) the dynamically generated BMP by image processing; and image (d) is an overlay of image (a) & (c) to demonstrate the accuracy.

3.3.2 Suspended Particle Detection

The first step in the process of adaptive encapsulation is to detect the particles suspended in the pre polymer resin. For the detection of the particles, we replicated the transmission mode of a simple microscope by using a white light source with a band-pass filter of center wavelength 532 nm from Thorlabs (Newton, NJ, USA) and a USB camera from Motic

(Xiamen, China) coupled with a 10X objective lens. The USB camera controlled by a LabVIEW module was used to capture images of the particles suspended in the pre polymer resin. The captured images were then taken as input to a MatLAB code written using the image-processing module. The captured raw images are first converted into binary images, the binary images are then used to find the location and radii of the suspended beads with the help of "imfindcircles" function from the MATLAB image-processing library, which is based on the Circular Hough Transform (CHT) algorithm.

3.3.3 Adaptive Particle Encapsulation using SFL

Using the advantage of generating a dynamic mask for the UV projection using a digital mirror device here, we demonstrate our capability of adaptively encapsulating polystyrene micro-beads.

Figure 3.19 shows the important process steps for the adaptive encapsulation of micro beads. First, a USB camera is used to capture images of the suspended particles in the microfluidic channel. The captured images are then converted into a binary image using "imbinarize" function in the image-processing module of MATLAB. To map pixel to pixel of the captured image to that of the DMD^{TM} the resize factor, magnification factor, translation pixel distances and rotation angle are used which were obtained as explained in section 3.3.1.
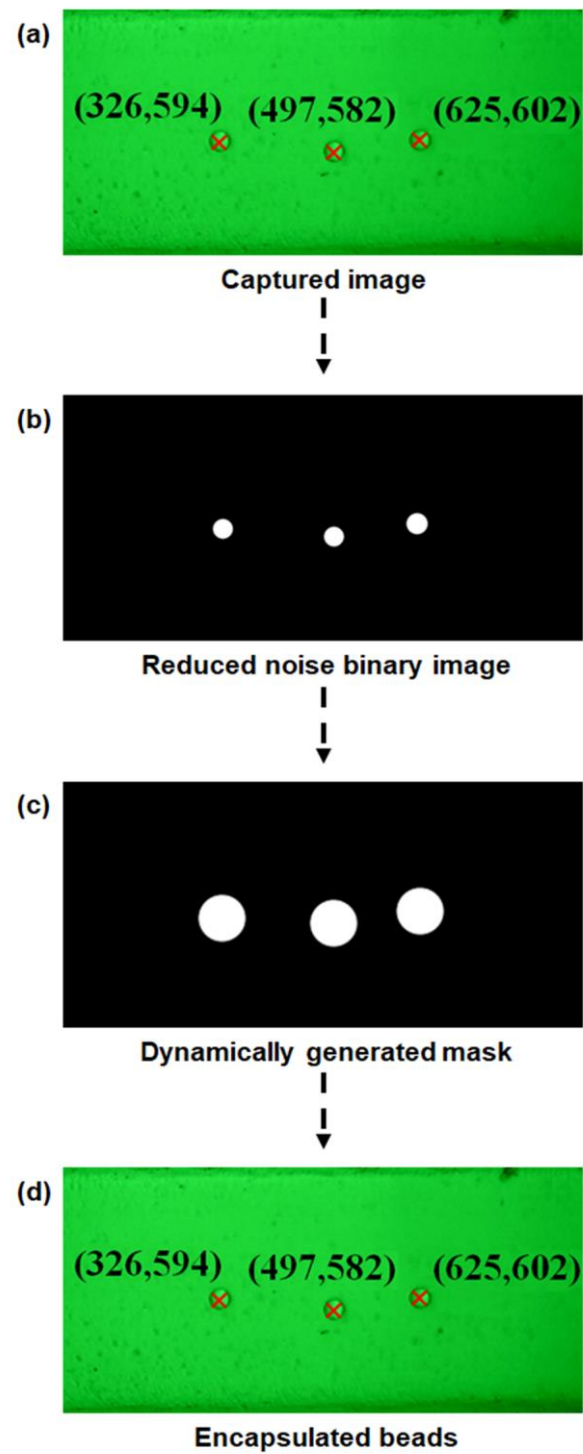
Figure 3.19: Adaptive encapsulation process steps; (a) captured raw image, (b) binary image after noise reduction, (c) dynamically generated BMP after image processing and (d) encapsulated micro beads.
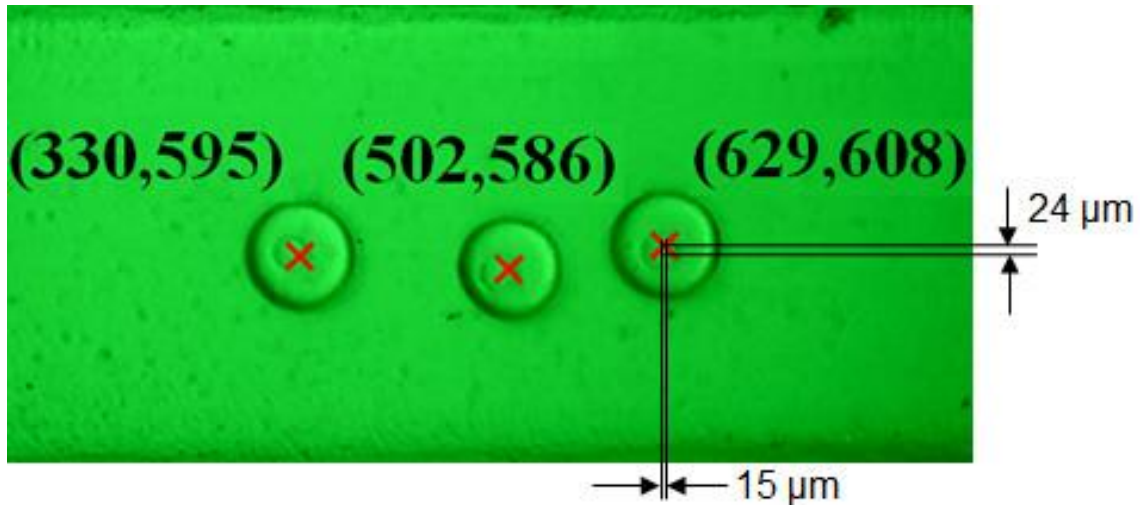
Figure 3.20: Adaptive encapsulation error analysis.

As seen in the figure the micro-beads have been successfully encapsulated. The coordinates on image (a) are the centers of the microbeads detected on the image, while the coordinates on image (d) are the centers of the printed structure. A slight misalignment between the beads and the printed structures can be observed. The miss-alignment is about 15 µm in X-direction and about 24 µm in Y-direction. This miss-alignment is attributed to the flow fluctuations between the process of capturing the image of the beads and projecting the UV pattern using the dynamically generated BMP to cure the polymer.

The technique of hydrodynamic focusing was used to align the micro particles in a single stream at the center of the channel. Hydrodynamic focusing occurs when multiple flows with substantially different flow rates come into contact. In a 3-inlet configuration, the center flow stream is pinched between two sheath streams, thereby shrinking the core stream width. With the sheath streams being wider than the core stream the level in the reservoir for the sheath streams drops quicker than the core stream over the period of time.

Moreover, the concept of hydraulic head is relied upon to stop the flow when the pressure is cut off. For the flow to become stagnant when the pressure is cut off the height of the polymer in the inlet and outlet reservoirs has to be same.

By depending on the hydraulic heads at the inlet and outlet reservoir to regulate the flow and hydrodynamic focusing to align the micro particles in the channel there is always a slight back-flow or forward flow that causes the beads to displace from the position of image acquisition. This results in a slight misalignment during encapsulation.
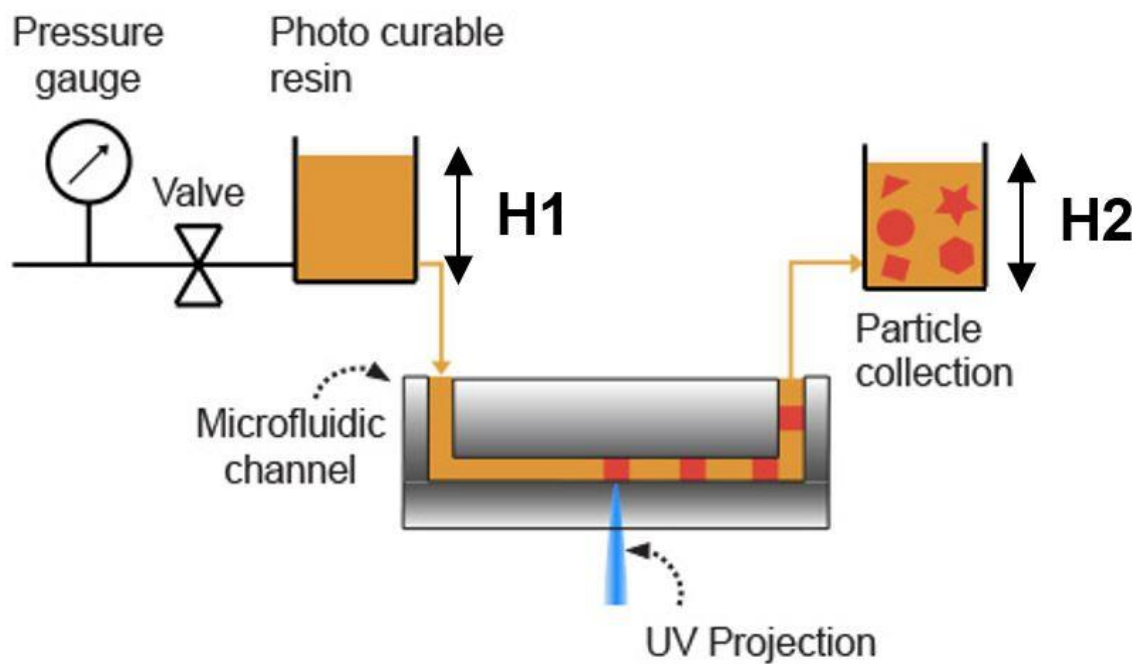
Figure 3.21: Schematic illustrating pressure head at inlet and outlet reservoirs.

- H1 = H2 Fluctuation free.
- H1 < H2 Back flow.
- H1 > H2 Forward flow.

Figure 3.22, demonstrates the concept of adaptive encapsulation by creating a cage around the particles and encapsulating the cells using a square structure. Highlighting our capability of single particle encapsulation, control over shape and size which would further allow one to tag information to the synthesized particle and assemble different shaped micro-particles to form larger architectures. The idea of single particle encapsulation can be extended to single cell encapsulation, which is of paramount importance in the field of cancer research, development biology and stem cell study.
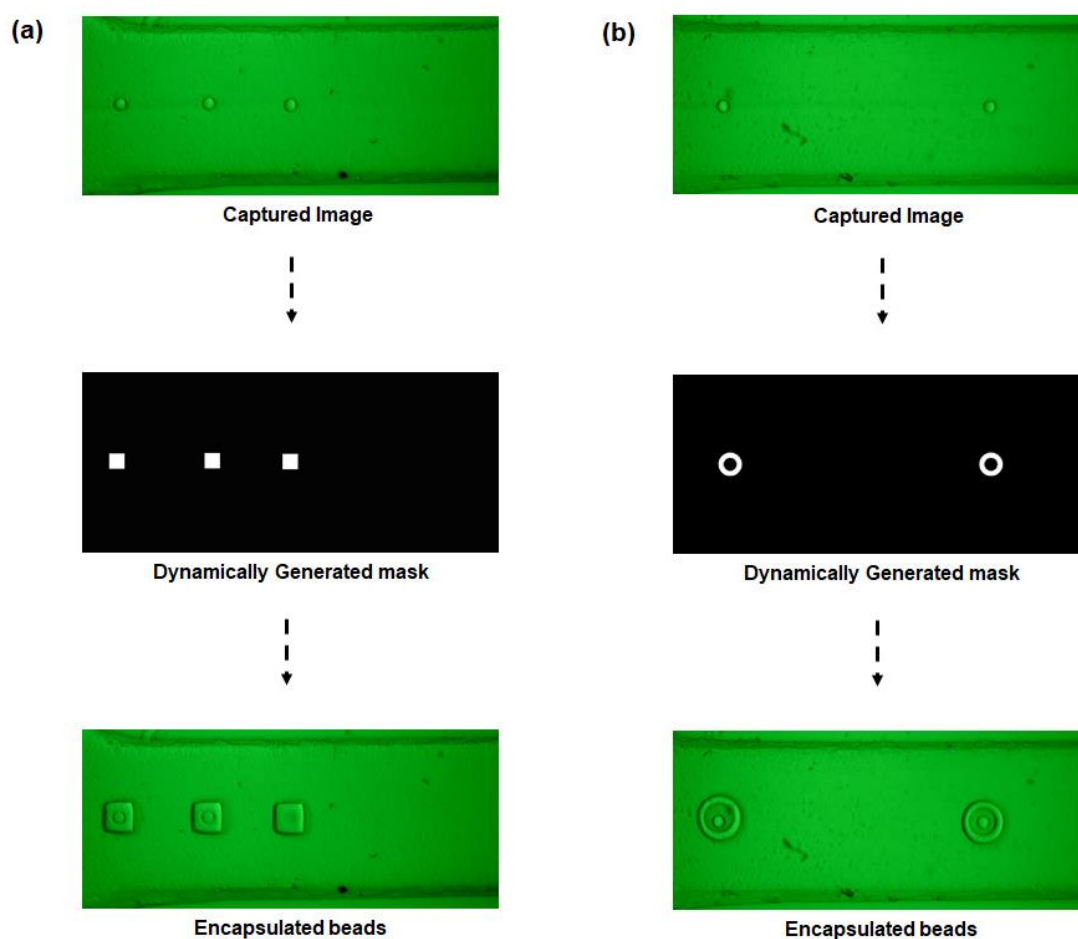
Figure 3.22: Adaptive encapsulation demonstration: Image (a) shows the encapsulation of the micro beads using a square structure &image (b) shows the caging of the micro beads using a ring.

Encapsulation Analysis:

To analyze the particle encapsulation process we captured a 20-second duration video of the particle encapsulation, determined the algorithm and system efficiency by counting the number of captured, and uncaptured suspended micro beads, and overlapped encapsulates were also considered. Not all the suspended micro beads stop in the field of view during the cycles and these micro beads, which do not stop in the field of view are considered to determine the system efficiency. The analysis results are tabulate in the table 3.9 below.

Figure 3.23: Sample image showing overlapped encapsulates and uncaptured micro beads.

Total number of particles (N)	Captured particles (NC)	Uncaptured particles (UC)	Overlapped particles (OP)	Algorithm efficiency (NC)/(NC+UC+OP)	System efficiency (NC)/(N)
87	23	11	3	58.8 %	26.4 %

Table 3.9: Particle encapsulation analysis result.

4 Conclusion

In this thesis, we present a system that combines high throughput fabrication and adaptive encapsulation of particles. This system is capable of producing particles with a feature size of ~200µm at a rate of ~3500 particles/hour with high control over size and shape, which play an important role in drug screening and tissue engineering. Unlike conventional "lithography" systems, our dynamic mask capability allows one to produce different particles in every cycle. Moreover, any photo curable functional materials can be used to produce particles with different mechanical properties.

We demonstrate adaptive particle encapsulation with the help of DMD^{TM} based dynamic mask by encapsulating polystyrene micro beads, which can easily be extended to encapsulating cells. We demonstrate single particle encapsulation overcoming the limitations of previous cell encapsulation processes. In addition to that, our dynamic mask capability can be used to tag data to the encapsulated particle, which is highly useful in biological, and bio medical engineering, cancer research, drug screening and stem cell study.

As a whole, the fabrication and particle encapsulation methodology developed here holds great promise in the field of cell proliferation, drug screening, and metastasis at the single-cell level.

Appendix A

MatLAB code for Scaling, Translation and Rotation:

```matlab
Capturedimg = imread('Capture1.jpg'); %Captured Image

gmat = Capturedimg(:,:,2);

i2 = im2bw(gmat,0.30); %Threshold conversion

i2 = imcomplement(i2);

ifilled = imfill(i2,'holes');

se = strel('disk',10);

iopenned = imopen(ifilled,se); %noise reduction

htest = zeros(800,1280,'uint8'); %Digital mask resolution canvas

[centers,radii,metric] = imfindcircles(iopenned,[30 80]);

[radius]= radii;

cr = [centers radius];

jtest = insertShape(htest,

'filledcircle',cr,'color',{'white'},'Opacity', 1);

originalbmp = imread('chemnewalignment25.bmp'); %original reference bmp

original = rgb2gray(originalbmp);

distorted = rgb2gray(jtest);

BW=edge(distorted,'prewitt');

[centers2, radii2, metric] = imfindcircles(BW,[30 80]);

BM=edge(original,'prewitt');

[centers1, radii1, metric] = imfindcircles(BM,[6 15]);

XX = centers1(6,1)- centers1(1,1); %from the bmp image

YY = centers2(5,1)- centers2(2,1); % from the captured image

resizefactorx = XX/YY;

zz = centers1(3,2)- centers1(1,2); %from the bmp image

ww = centers2(8,2)- centers2(2,2); %from the captured image

resizefactory = zz/ww;
```

```matlab
resizefactor = max(resizefactorx,resizefactory);

d = imresize(jtest,resizefactor,'Method','nearest'); %resizing image

distorted2 = rgb2gray(d);

Bx=edge(distorted2,'prewitt');

[centers3, radii3, metric] = imfindcircles(Bx,[15 40]);

cr3 = [centers3 radii3];

% plotting circles on the Digital mask resolution canvas

distortedtest = insertShape(htest,

'filledcircle',cr3,'color',{'white'},'Opacity', 1);

translationX = centers1(1,1) - centers3(7,1);

translationY = centers1(1,2) - centers3(7,2);

ZR1 = mean2(radii1);

ZR3 = mean2(radii3);

ZFR = ZR1/ZR3; %Magnification factor

[radius]= radii3*ZFR;

[mn nm] = size(centers3);

for z = 1:mn

    centers4(z,1) = centers3(z,1)+ (translationX - 0.5);

    centers4(z,2) = centers3(z,2)+ (translationY + 1.5);

end

cr = [centers4 radius];

blank = zeros(800,1280,'uint8'); %Digital mask resolution canvas

jjj = insertShape(blank,

'filledcircle',cr,'color',{'white'},'Opacity',1);

JJ = imrotate(jjj,-2.5,'bilinear','crop'); %image rotation

imwrite(JJ, 'finaltest.bmp');

zh = imfuse(original,JJ); %overlaying images for comparision

figure, imshow(zh);

imwrite(zh, 'overlay.bmp');
```

Appendix B

MatLAB code for Circular encapsulation:

```matlab
clear centers, clear centers3, clear radii3, clear radii;

ZF = 0.3711; %Resize factor

ZFR = 0.8240; %Magnification factor

translationX = 403.6185; %xtranslation

translationY = 208.8922; %ytranslation

Rotation = -1; %angle of rotation

bm =

strcat('C:\Users\3D_PuSL\Desktop\manish\cellencapsulation\10152017\capt

ured\Test', num2str(X), '.bmp');

b = imread(bm);

gmat = b(:,:,2);

i2 = im2bw(gmat,0.57); %Threshold conversion

i2 = imcomplement(i2);

ifilled = imfill(i2,'holes');

se = strel('disk',1);

iopenned = imopen(ifilled,se); %noise reduction

h = zeros(800,1280,'uint8'); %Digital mask resolution canvas

[centers,radii,metric] = imfindcircles(iopenned,[12 35]);

[kb sb] = size(centers);

radius = [];

cr = [];

if kb > 0

    [radius]= radii;

    cr = horzcat(centers,radius);

    j = insertShape(h,

'filledcircle',cr,'color',{'white'},'Opacity',1);
```

```matlab
    d = imresize(j,ZF,'Method','nearest'); %resizing the image

    distorted = rgb2gray(d);

    Bx=edge(distorted,'prewitt');

    [centers3, radii3, metric] = imfindcircles(Bx,[6 15]);

    centers4 = [];

    radius3 = [];

    [radius3]= (radii3*ZFR)+10; %radius of the encapsulate

    [mn nm] = size(centers3);

    for z = 1:1:mn

        centers4(z,1) = centers3(z,1)+ (translationX - 20);

        centers4(z,2) = centers3(z,2)+ (translationY - 65);

    end

    cr1 = [];

    cr1 = horzcat(centers4,radius3);

    jjj = insertShape(h,
'filledcircle',cr1,'color',{'white'},'Opacity', 1); %after translation

    JJ = imrotate(jjj,Rotation,'bilinear','crop'); %image rotation

    %cropping the generated BMP to remove surrounding noice

    croprect = [580 0 149 800];

    crop_1 = imcrop(JJ,croprect);

    crop_1 = rgb2gray(crop_1);

    cropsize = size(crop_1);

    cropxspan = cropsize(1,2);

    cropyspan = cropsize(1,1);

    blank2 = zeros(800,1280,'uint8');

    for czx = 580:1:580+cropxspan-1

        for czy = 1:1:cropyspan-1

            blank2(czy,czx)= crop_1(czy,czx-(580-1));

        end
```

```matlab
    end

    mb =

strcat('C:\Users\3D_PuSL\Desktop\manish\cellencapsulation\10152017\bmp\

bmp', num2str(X), '.bmp');

    imwrite(blank2, mb,'bmp'); %saving the dynamically generated mask


else

    blank = zeros(800,1280,'uint8');

    nb =

strcat('C:\Users\3D_PuSL\Desktop\manish\cellencapsulation\10152017\bmp\

bmp', num2str(X), '.bmp');

    imwrite(blank, nb,'bmp');

end
```

Appendix C

MatLAB code for Square encapsulation:

```
clear centers, clear centers3, clear radii3, clear radii;
ZF = 0.3711; %Resize factor
ZFR = 0.8240; %Magnification factor
translationX = 403.6185; %xtranslation
translationY = 208.8922; %ytranslation
Rotation = -1; %angle of rotation
bm =
strcat('C:\Users\3D_PuSL\Desktop\manish\cellencapsulation\10152017\capt
ured\Test', num2str(X), '.bmp');
b = imread(bm);
gmat = b(:,:,2);
i2 = im2bw(gmat,0.57); %Threshold conversion
i2 = imcomplement(i2);
ifilled = imfill(i2,'holes');
se = strel('disk',1);
iopenned = imopen(ifilled,se); %noise reduction
h = zeros(800,1280,'uint8'); %Digital mask resolution canvas
[centers,radii,metric] = imfindcircles(iopenned,[12 35]);
[kb sb] = size(centers);
radius = [];
cr = [];
if kb > 0
    [radius]= radii;
    cr = horzcat(centers,radius);
    j = insertShape(h, 'filledcircle',cr,'color',{'white'},'Opacity',
1);
```

```matlab
d = imresize(j,ZF,'Method','nearest'); %resizing the image

distorted = rgb2gray(d);

Bx=edge(distorted,'prewitt');

[centers3, radii3, metric] = imfindcircles(Bx,[6 15]);

centers4 = [];

radius3 = [];

[radius3]= (radii3*ZFR)+10; %radius of the encapsulate

[mn nm] = size(centers3);


for z = 1:1:mn

    centers4(z,1) = centers3(z,1)+ (translationX - 20);

    centers4(z,2) = centers3(z,2)+ (translationY - 65);

end

cr1 = [];

cr1 = horzcat(centers4,radius3);

jjj = insertShape(h,
'filledcircle',cr1,'color',{'white'},'Opacity', 1); %after translation

JJ = imrotate(jjj,Rotation,'bilinear','crop'); %image rotation

%cropping the generated BMP to remove surrounding noice

croprect = [580 0 149 800];

crop_1 = imcrop(JJ,croprect);

crop_1 = rgb2gray(crop_1);

cropsize = size(crop_1);

cropxspan = cropsize(1,2);

cropyspan = cropsize(1,1);

blank2 = zeros(800,1280,'uint8');

for czx = 580:1:580+cropxspan-1

    for czy = 1:1:cropyspan-1
```

```matlab
                blank2(czy,czx)= crop_1(czy,czx-(580-1));
        end
    end
    mb =
strcat('C:\Users\3D_PuSL\Desktop\manish\cellencapsulation\10152017\bmp\
bmp', num2str(X), '.bmp');
    imwrite(blank2, mb,'bmp'); %saving the dynamically generated mask
    %inserting the square library image


squareimage=imread('C:\Users\3D_PuSL\Desktop\manish\cellencapsulation\s
quareimage\square.bmp');%replacing circles with squares
    microsphere= blank2;
    finalbmp = zeros(800,1280);
    sqcenters = [];
    sqradii = [];
    [sqcenters,sqradii,metric] = imfindcircles(microsphere,[15 45]);
    imgsize = size(squareimage);
    [smn snm] = size(sqcenters);
    yspan = imgsize(1,2);
    xspan = imgsize(1,1);
    for sz = 1:1:smn
        xini = round(sqcenters(sz,2));
        yini = round(sqcenters(sz,1));
        for p=xini-xspan/2:xini+xspan/2-1
            for k=yini-yspan/2:yini+yspan/2-1


                finalbmp(p,k)=squareimage(p-xini+xspan/2+1,k-
yini+yspan/2+1);
```

```matlab
            end

        end

    end

    finalbmpaddress =

strcat('C:\Users\3D_PuSL\Desktop\manish\cellencapsulation\10152017\bmp\

bmp', num2str(X), '.bmp');

    imwrite(finalbmp, finalbmpaddress,'bmp'); %Final Dynamically

generated mask

else

    blank = zeros(800,1280);

    nb =

strcat('C:\Users\3D_PuSL\Desktop\manish\cellencapsulation\10152017\bmp\

bmp', num2str(X), '.bmp');

    imwrite(blank, nb,'bmp');

end
```

Appendix D

MatLAB code for Caging:

```matlab
clear centers, clear centers3, clear radii3, clear radii;

ZF = 0.3711; %Resize factor

ZFR = 0.8240; %Magnification factor

translationX = 403.6185; %xtranslation

translationY = 208.8922; %ytranslation

Rotation = -1; %angle of rotation

bm =

strcat('C:\Users\3D_PuSL\Desktop\manish\cellencapsulation\10152017\capt

ured\Test', num2str(X), '.bmp');

b = imread(bm);

gmat = b(:,:,2);

i2 = im2bw(gmat,0.57); %Threshold conversion

i2 = imcomplement(i2);

ifilled = imfill(i2,'holes');

se = strel('disk',1);

iopenned = imopen(ifilled,se); %noise reduction

h = zeros(800,1280,'uint8'); %Digital mask resolution canvas

[centers,radii,metric] = imfindcircles(iopenned,[12 35]);

[kb sb] = size(centers);

radius = [];

cr = [];

if kb > 0

    [radius]= radii;

    cr = horzcat(centers,radius);

    j = insertShape(h, 'filledcircle',cr,'color',{'white'},'Opacity',

1);
```

```matlab
d = imresize(j,ZF,'Method','nearest'); %resizing the image

distorted = rgb2gray(d);

Bx=edge(distorted,'prewitt');

[centers3, radii3, metric] = imfindcircles(Bx,[6 15]);

centers4 = [];

radius3 = [];

[radius3]= (radii3*ZFR)+10; %radius of the encapsulate

[mn nm] = size(centers3);


for z = 1:1:mn

    centers4(z,1) = centers3(z,1)+ (translationX - 20);

    centers4(z,2) = centers3(z,2)+ (translationY - 65);

end

cr1 = [];

cr1 = horzcat(centers4,radius3);

jjj = insertShape(h, 'circle',cr1, 'LineWidth',
10,'color',{'white'}); %after translation

JJ = imrotate(jjj,Rotation,'bilinear','crop'); %image rotation

%cropping the generated BMP to remove surrounding noice

croprect = [580 0 149 800];

crop_1 = imcrop(JJ,croprect);

crop_1 = rgb2gray(crop_1);

cropsize = size(crop_1);

cropxspan = cropsize(1,2);

cropyspan = cropsize(1,1);

blank2 = zeros(800,1280,'uint8');

for czx = 580:1:580+cropxspan-1

    for czy = 1:1:cropyspan-1
```

```matlab
            blank2(czy,czx)= crop_1(czy,czx-(580-1));

        end

    end

    mb =
strcat('C:\Users\3D_PuSL\Desktop\manish\cellencapsulation\10152017\bmp\
bmp', num2str(X), '.bmp');

    imwrite(blank2, mb,'bmp'); %saving the dynamically generated mask
else

    blank = zeros(800,1280);

    nb =
strcat('C:\Users\3D_PuSL\Desktop\manish\cellencapsulation\10152017\bmp\
bmp', num2str(X), '.bmp');

    imwrite(blank, nb,'bmp');

end
```

References

[1] Urban, Dieter, and Koichi Takamura, eds. Polymer dispersions and their industrial applications. Weinheim: Wiley-VCH, 2002.

[2] Dendukuri, Dhananjay, and Patrick S. Doyle. "The synthesis and assembly of polymeric microparticles using microfluidics." Advanced Materials 21.41 (2009): 4071-4086.

[3] Kim, Shin-Hyun, Seog-Jin Jeon, and Seung-Man Yang. "Optofluidic encapsulation of crystalline colloidal arrays into spherical membrane." Journal of the American Chemical Society 130.18 (2008): 6040-6046.

[4] Kawakatsu, Takahiro, Yuji Kikuchi, and Mitsutoshi Nakajima. "Regular-sized cell creation in microchannel emulsification by visual microprocessing method." Journal of the American Oil Chemists' Society 74.3 (1997): 317-321.

[5] Thorsen, Todd, et al. "Dynamic pattern formation in a vesicle-generating microfluidic device." Physical review letters 86.18 (2001): 4163.

[6] Anna, Shelley L., Nathalie Bontoux, and Howard A. Stone. "Formation of dispersions using "flow focusing" in microchannels." Applied physics letters 82.3 (2003): 364-366.

[7] Jeong, Won Je, et al. "Continuous fabrication of biocatalyst immobilized microparticles using photopolymerization and immiscible liquids in microfluidic systems." Langmuir 21.9 (2005): 3738-3741.

[8] Sugiura, Shinji, et al. "Preparation of monodispersed solid lipid microbeads using a microchannel emulsification technique." Journal of colloid and interface science 227.1 (2000): 95-103.

[9] Sugiura, Shinji, et al. "Synthesis of polymeric microbeads with narrow size distributions employing microchannel emulsification." Macromolecular rapid communications 22.10 (2001): 773-778.

[10] Nisisako, Takasi, Toru Torii, and Toshiro Higuchi. "Novel microreactors for functional polymer beads." Chemical Engineering Journal 101.1 (2004): 23-29.

[11] Sugiura, Shinji, et al. "Size control of calcium alginate beads containing living cells using micro-nozzle array." Biomaterials 26.16 (2005): 3327-3331.

[12] Tan, W-H., and Shoji Takeuchi. "Monodisperse alginate hydrogel microbeads for cell encapsulation." Advanced Materials 19.18 (2007): 2696-2701.

[13] Dendukuri, Dhananjay, et al. "Controlled synthesis of nonspherical microparticles using microfluidics." Langmuir21.6 (2005): 2113-2116.

[14] Dendukuri, Dhananjay, et al. "Continuous-flow lithography for high-throughput microparticle synthesis." Nature materials 5.5 (2006).

[15] Dendukuri, Dhananjay, et al. "Stop-flow lithography in a microfluidic device." Lab on a Chip 7.7 (2007): 818-828.

[16] Decker, Christian, and Aubrey D. Jenkins. "Kinetic approach of oxygen inhibition in ultraviolet-and laser-induced polymerizations." Macromolecules 18.6 (1985): 1241-1244.

[17] Chung, Su Eun, et al. "Optofluidic maskless lithography system for real-time synthesis of photopolymerized microstructures in microfluidic channels." Applied Physics Letters 91.4 (2007): 041106.

[18] Chung, Su Eun, et al. "Guided and fluidic self-assembly of microstructures using railed microfluidic channels." Nature materials 7.7 (2008): 581-587.

[19] Pregibon, Daniel C., Mehmet Toner, and Patrick S. Doyle. "Multifunctional encoded particles for high-throughput biomolecule analysis." Science 315.5817 (2007): 1393-1396.

[20] Wang, Huanan, et al. "The use of micro-and Nano beads as functional components for bone tissue regeneration." Tissue Engineering Part B: Reviews 18.1 (2011): 24-39.

[21] Rowley, Jon A., Gerard Madlambayan, and David J. Mooney. "Alginate hydrogels as synthetic extracellular matrix materials." Biomaterials 20.1 (1999): 45-53.

[22] Choi, Chang-Hyung, et al. "One-step generation of cell-laden microgels using double emulsion drops with a sacrificial ultra-thin oil shell." Lab on a Chip 16.9 (2016): 1549-1555.

[23] Panda, Priyadarshi, et al. "Stop-flow lithography to generate cell-laden microgel particles." Lab on a Chip 8.7 (2008): 1056-1061.

[24] Chung, Su Eun, et al. "Optofluidic encapsulation and manipulation of silicon microchips using image processing based optofluidic maskless lithography and railed microfluidics." Lab on a Chip 9.19 (2009): 2845-2850.

[25] Bong, Ki Wan, et al. "Compressed-air flow control system." Lab on a Chip 11.4 (2011): 743-747.

[26] Decker, Christian, and Aubrey D. Jenkins. "Kinetic approach of oxygen inhibition in ultraviolet-and laser-induced polymerizations." *Macromolecules* 18.6 (1985): 1241-1244.